NASA Technical Paper 3586

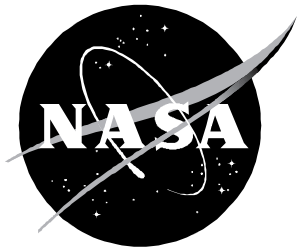

Quasi-Static and Dynamic Response Characteristics of F-4 Bias-Ply and Radial-Belted Main Gear Tires

Pamela A. Davis
Langley Research Center • Hampton, Virginia

National Aeronautics and Space Administration
Langley Research Center • Hampton, Virginia 23681-0001

February 1997

Available electronically at the following URL address: http://techreports.larc.nasa.gov/ltrs/ltrs.html

Printed copies available from the following:

NASA Center for AeroSpace Information
800 Elkridge Landing Road
Linthicum Heights, MD 21090-2934
(301) 621-0390

National Technical Information Service (NTIS)
5285 Port Royal Road
Springfield, VA 22161-2171
(703) 487-4650

Contents

Nomenclature

A	constant
A_{grooves}	tread groove area, in^2
A_{gross}	area of entire footprint, in^2
A_{net}	net footprint area, in^2
B	constant
c	damper constant
C	constant
C_c	critical damping constant
C_{eq}	equivalent viscous damping factor
E_{cyc}	energy dissipated per cycle, in-lb
f	frequency of oscillation, Hz
f_d	equivalent displacement, in.
F	external load applied to a system, lb
F_d	damping/friction force, lb
F_{max}	load at maximum deflection, lb
F_0	initial applied-force magnitude, lb
$F_{x=0}$	load at zero deflection, lb
J	mass moment of inertia, in-lb-sec^2
k	spring rate, lb/in.
k_c	spring rate from cable interaction, lb/in.
k_p	platen spring rate, lb/in.
k_t	tire spring rate, lb/in.
k/m	frequency parameter
L	length of support cables, ft
m	mass of system, lb_m
m_p	mass of platen, lb_m
r	radius of circle, in.
R	radial distance from center of plate to support cables, in.
t	time, sec
w_p	platen weight, lb
W	weight of object, lb
x	displacement, in.
X	maximum displacement amplitude, in.
α	acceleration, ft/sec^2
β	structural damping factor
Δ	increment of change
δ	log decrement
μ	friction coefficient
μ_k	kinetic friction coefficient

ϕ	phase angle of damped oscillation, deg
τ	period of oscillation, sec
θ	angle of circle, rad
ω	circular forcing frequency, Hz
ω_d	frequency of damped free vibration, Hz
ω_n	natural frequency of vibration, Hz
ζ	viscous damping factor

Abstract

An investigation was conducted at Langley Research Center to determine the quasi-static and dynamic response characteristics of the U.S. Air Force F-4 fighter 30×11.5-14.5/26PR bias-ply and radial-belted main gear tires. Tire properties were measured by the application of vertical, lateral, and fore-and-aft loads. Mass moment-of-inertia data were also obtained. The results of the study include quasi-static load-deflection curves, free-vibration time-history plots, energy loss associated with hysteresis, stiffness and damping characteristics, footprint geometry, and inertia properties of each type of tire. The difference between bias-ply and radial-belted tire construction is given, as well as the advantages and disadvantages of each tire design. Three simple damping models representing viscous, structural, and Coulomb friction are presented and compared with the experimental data. The conclusions that are discussed contain a summary of test observations. Results of this study show that radial-belted tire vertical stiffness values are comparable to the bias-ply tire stiffness and that use of this radial-belted tire on aircraft should not affect aircraft landing dynamics. Lateral and fore-and-aft stiffness properties were diminished in the radial-belted tire, thus leading to the possibility of increased tire shimmy and raising the question of compatibility with the existing antiskid braking system for this tire. Lateral and fore-and-aft damping were increased in the free-vibration tests when they were compared with damping from the quasi-static tests, suggesting not only the presence of the assumed structural damping but also the presence of viscous damping. Coulomb friction characteristics were not applicable to the tests that were conducted. Footprint geometrical data suggest that footprint aspect ratio effects may interfere with improved hydroplaning potential that is associated with this radial-belted tire that is operated at a higher inflation pressure than the bias-ply tire. Moment-of-inertia values were lower for the radial-belted tire than for its bias-ply counterpart; the lower values indicate that less energy is needed during spin-up operations and should result in less tread wear for this radial-belted tire.

Introduction

When the Wright brothers made their first flight in 1903, tires were not part of the design. The first wheeled landing-gear flight was made in Europe in October 1906 by Santos-Dumont's "No. 14 bis" aircraft (ref. 1). Since then the bias-ply aircraft tire has gone through many changes which have enhanced its performance. Thus, there has been little desire in the aircraft landing-gear industry to change from the bias-ply tire to the newer radial-belted tire. For more than 30 years (Europe in the 1960's and the United States in the 1970's), the automotive industry has found that radial-belted tires heighten vehicle performance and offer many advantages over the traditional bias-ply tire (ref. 2). Despite the benefits of radial-belted automotive tires (longer tread life, cooler operating temperatures, and improved friction characteristics), the general belief in the aircraft landing-gear industry, until 1980, was that the mechanical properties of these radial-belted tires were unacceptable for aircraft use. For example, landing-gear designers had several concerns about radial tires that included the following: (1) lateral forces during crosswind landings might exceed tire-wheel coupling capability, (2) tire fore-and-aft stiffness properties might degrade the performance characteristics of aircraft antiskid braking systems, and (3) greatly reduced tire vertical stiffness characteristics might adversely affect aircraft landing dynamic response.

Understandably, the aircraft tire industry cautiously approached the production of radial-belted tires. However, the idea that aircraft operating costs could be lowered by increasing tread life, reducing tire weight, and improving safety margins over the current bias-ply aircraft tire were sufficient reasons to continue efforts to achieve a radial-belted aircraft tire. Several tire manufacturers, both in Europe and in the United States, have developed radial-belted aircraft tire designs which appear to overcome many of the previously mentioned concerns and which have been successfully tested on several different aircraft. Today, radial-belted tires have been certified and are being used on commercial aircraft such as the Dassault Aviation Falcon 900, Airbus Industries aircraft, the French ATR 42 transport, and on military aircraft such as the U.S. Air Force F-15E, the French Mirage, and the British Tornado (ref. 3).

In order to analyze tire mechanical properties associated with aircraft takeoff, landing, and taxi operations, tire and landing-gear designers must have accurate, up-to-date tire data available. Still used extensively, NASA Technical Report R-64 by Smiley and Horne (ref. 4) summarizes the state of knowledge of the mechanical characteristics of aircraft tires as they existed over 30 years ago. Because this report deals exclusively with bias-ply tires, a need exists for a similar database of radial-belted aircraft tire mechanical properties for use in the prediction of landing-gear response characteristics for modern aircraft.

This research effort was initiated to study the mechanical properties of radial-belted and bias-ply 30×11.5-14.5/26PR aircraft tires (the main gear tire on the U.S. Air Force F-4 fighter) under a variety of test conditions and to develop a radial-belted tire properties database. In this investigation, the bias-ply tire was tested at the rated inflation pressure of 245 psi, and the radial-belted tire was tested at 310 psi. These inflation pressures correspond to a 35-percent tire vertical deflection at the rated vertical load of 25 000 lb. Both tires have a 26-ply rating. The two tire types used in this investigation are shown, uninflated and unmounted, in figure 1, and their principal characteristics are given in table 1. All tires were furnished by the U.S. Air Force and were procured from different tire manufacturers. Prior to testing by the National Aeronautics and Space Administration (NASA), all tires were preconditioned at the Wright Research Development Center, Dayton, Ohio with 2 miles of taxi tests at 26 knots at rated load and inflation pressure.

The objectives of the work presented here are (a) to determine, to evaluate, and to compare certain quasi-static and dynamic response characteristics of the 30×11.5-14.5/26PR aircraft main gear tire of a bias-ply and a radial-belted design; (b) to use these properties to help define tire performance during taxi, takeoff, and landing operations; and (c) to define the suitability of the radial-belted tire as a replacement for the bias-ply aircraft tire. To accomplish these objectives, vertical, lateral, fore-and-aft, and inertial tire properties were determined, as well as the type of damping that was present during static and dynamic testing. The study involved the following tasks:

1. Measurement of vertical, lateral, and fore-and-aft load deflection, stiffness and hysteretic properties of each tire type
2. Measurement of tire footprint geometrical and inertial properties
3. Definition of viscous, structural, and Coulomb friction damping models
4. Application of these simple damping models to the two tire designs tested
5. Comparison and analysis of experimental test results

Review of Previous Pertinent Work

From the simple horsedrawn cart to the high-speed transport aircraft of today, wheels and tires have become an essential part of our transportation system. As a result, landing-gear designers and engineers have been optimizing methods of defining tire mechanical properties and solving such problems as landing-gear vibration, tire wear, and tire heating. A major contribution to the landing-gear industry, which set the standard for analytically defining tire properties, was a publication by Smiley and Horne (ref. 4) on mechanical properties of pneumatic tires. The database for NASA Report R-64, however, was various sizes of bias-ply pneumatic tires only.

Tanner (ref. 5) did early testing with radial-belted aircraft tires in 1974 in which he defined tire fore-and-aft elastic characteristics and noted lower tread wear and heat dissipation for the radial-belted tire compared with bias-ply and bias-belted tires. He also concluded that the lower fore-and-aft stiffness properties of the radial-belted tire, compared with the bias-ply tire, could have an impact on aircraft antiskid system performance. Tire manufacturers published some of their findings on radial-belted tire characteristics in the 1980's. The data presented were limited but invaluable to tire designers and engineers (refs. 6–8). Both NASA and the U.S. Air Force have taken the lead in quasi-static and dynamic testing of radial-belted aircraft tires. References 5–20 compare the properties of radial-belted and bias-ply aircraft tires. These publications have helped aircraft tire manufacturers optimize the radial-belted design.

In addition to defining tire mechanical properties, there has been interest in the damping characteristics of aircraft tires, especially radial-belted tires. Shimmy is a problem for aircraft landing gear just as it is for the front end of automobiles. Shimmy, defined as the self-excited oscillation of wheels about their axis, was evaluated early in aviation history for aircraft nose gear by Von Schlippe and Dietrich (refs. 21 and 22) and later by Moreland (ref. 23), de Carbon (ref. 24), and Collins and Black (refs. 25 and 26). Although these theories do require certain tire properties such as static lateral stiffness and the viscous damping factor to be initially determined, none completely addresses the issue of tire damping and its contributions to landing-gear shimmy behavior. Many works have been published that address structural (hysteretic) and viscous damping (refs. 4, 11–13, 19, and 27–34), but few tire analysts have used these developed models to define precisely the damping

mechanism in the tire-wheel assembly under both quasi-static and dynamic test conditions.

Construction of Bias-Ply and Radial-Belted Aircraft Tires

The aircraft tire is a mechanical system that has three primary functions: (1) to provide lateral stability to the aircraft by the generation of lateral forces while under deformation, (2) to act as a mechanical buffer and shock absorber while under load and in contact with the ground, and (3) to provide a mechanism for braking to reduce ground speed (ref. 35).

The generation of lateral forces is an important function of the aircraft tire. As an airplane approaches a runway, it is supported laterally in the air and can approach at an angle in a crosswind. Airplane aerodynamics continue to provide lateral support to the aircraft at touchdown where a minimum lateral tire force is required. The maximum lateral force from the tires is required as the aircraft slows down during rollout and during taxi operations. Thus, aircraft tire manufacturers had to design a radial-belted tire that would not generate lateral forces that were too high during touchdown, which, in turn, could cause lateral instability that would transmit high loads to the landing gear (ref. 7).

While acting as a buffer and shock absorber for the aircraft during the landing impact, the tire must also be able to carry extremely heavy loads at high speeds. A race car tire may require this speed capability, but compared with an aircraft tire, a race car tire is lightly loaded. In contrast, military and commercial aircraft operate at high speeds but can be loaded up to 50 000 lb per tire.

During braking the tire must be able to reduce ground speed while surviving within and resisting environmental factors to decelerate the aircraft (ref. 8). Environmental factors influenced by weather are snow, ice, and rain; factors that result from runway conditions are bumps, potholes, and foreign objects.

The following sections describe the design of the bias-ply and radial-belted aircraft tires, examine the differences between the two tire types, and highlight the unique radial-belted design.

Bias-Ply Aircraft Tires

The bias-ply tire is constructed of numerous laminates of rubber-textile plies that alternate at various angles from 60° near the wire beads to 30° near the crown area of the tire (fig. 2). Additional plies are laid at some specified angle between the tire carcass and the tread to provide tread reinforcement. Multiple bead wires on each side of the tire hold together the large number of plies and form a torus-like shell. The highly stiffened shell and the weight of the tire are a result of the ply assembly and the multiple-ply casing. At the bead heel, chaffer strips are added for additional protection. Because of its cross-ply construction, the bias-ply tire has greater interply friction than its radial-belted tire counterpart, which leads to significant structural stresses during tire flexing. These stresses result in severe heat buildup in the tire casing and tread rubber during ground operations. This heat buildup can be limited by adding reinforcing plies, but at the expense of additional weight. The size of the bias-ply tire required for an aircraft application is determined by both the load-carrying requirements and the acceptable tire pressure (ref. 7).

Radial-Belted Aircraft Tires

The radial-belted aircraft tire has carcass plies approximately oriented in the plane of the tire cross section (fig. 3). Its size and load-carrying requirements determine the number of plies in the tire. Fewer plies of higher denier textile cords result in a weight and volume savings over the comparable bias-ply tire. The weight and volume savings result in an increase in payload for commercial aircraft and an increase in armament for military aircraft. For the radial-belted tire tested in this research effort, there was a 20-percent weight savings over the bias-ply tire. Generally, only one steel-bead wire is needed on each side of the tire, as opposed to multiple bead wires in the bias-ply tire. For the radial-belted tires used in this investigation, a textile cord belt surrounds the casing of the tire circumferentially, and a woven steel belt surrounds the cord belt and acts as a protector ply. The separation of the casing and belt package contributes to the uniqueness of the radial-belted tire. When the casing flexes under load, the tread is stabilized by the belt package, and there is less tire scrubbing (lateral sliding of the tire on the pavement). Shear stresses in the rubber matrix are minimized, and loads are efficiently distributed throughout the tire structure. There is less interply friction and thus less heat buildup during ground operations. Therefore, the radial-belted tire can have a layer of unreinforced wear rubber (no reinforcing plies) beneath the tread. This design reduces the tendency of the tire to chunk and increases its wear resistance. (See refs. 2, 3, 5, 7, 8, 14, and 35.)

Test Apparatus and Procedures

Quasi-static pure vertical-loading tests, combined vertical-lateral loading tests, and combined vertical fore-and-aft loading tests were conducted to measure tire load-deflection properties, spring-rate values, damping factors, and energy loss associated with hysteresis. Footprint geometrical properties for the two tire designs were also measured. Free-vibration tests of combined

vertical-lateral and vertical fore-and-aft tests were completed to measure tire stiffness values, damping characteristics, and energy loss associated with damped harmonic motion. Finally, moment-of-inertia tests were obtained for each tire type.

The bias-ply tire was tested at an inflation pressure of 245 psi, and the radial-belted tire was tested at an inflation pressure of 310 psi. The inflation pressures correspond to a 35-percent tire vertical deflection at the rated vertical load of 25 000 lb. An inflation pressure of 245 psi for the radial-belted tire yielded a 52-percent tire deflection. Although it is preferable to compare tires at the same inflation pressure, it was more important that they be tested at the same percent tire deflection because this percentage is a major requirement for tire mixability on landing gear. An increase in tire deflection can cause tire overheating. Tests were conducted on the radial-belted tire at the lower inflation pressure of 245 psi, and the results indicate greatly reduced quasi-static and dynamic mechanical properties. References 11 and 20 contain further information and data on these tests at the lower inflation pressure of 245 psi for this radial-belted tire design. The following sections describe the test apparatus and procedures used to obtain the desired tire properties.

Test Apparatus No. 1

The test apparatus used to measure the tire vertical mechanical properties under quasi-static loading conditions is shown in figure 4. The tire wheel-axle assembly is mounted on a dynamometer that is instrumented with five strain-gauge beams. Two beams are used for measuring vertical load and two are used for fore-and-aft load; one beam is used for measuring lateral load. The test fixture has one hydraulic cylinder which applies vertical load to the dynamometer and loads the tire onto the surface of a 40-in-square frictionless table or bearing plate. The table is instrumented with three load cells mounted underneath to measure the applied vertical load. Each load cell has a span of 0 to 50 000 lb with a loading accuracy of ±30 lb. A displacement transducer is mounted parallel to the hydraulic cylinder to measure tire vertical displacements. The displacement transducer has a span of 0 to 5.5 in. with a measuring accuracy of ±0.02 in.

For the quasi-static pure vertical-load tests, load was applied hydraulically to the tire until the maximum rated vertical load of 25 000 lb was reached; the applied load was then gradually reduced to zero. Output data from the various instruments were recorded by a computer in 1000-lb increments for these tests. Measurements were taken at four different peripheral positions around each tire. Vertical load and deflection were continuously monitored during the loading and unloading cycle to produce a load-deflection curve or hysteresis loop. Such data provided an indication of tire vertical-loading behavior and defined the vertical spring rate and energy loss characteristics. Subsequent to the tests, the data were converted into engineering units and saved for further analysis and evaluation.

Test Apparatus No. 2

A second test apparatus used for quasi-static and free-vibration lateral and fore-and-aft load tests is shown schematically in figure 5. It consists of a main structure with two three-bay portal frames joined overhead by four beams and along the floor by a thick plate. The tire-wheel assembly is mounted between two aluminum adapter plates which are each fixed to a vertical beam suspended from the upper part of the structure. The adapter plates prevent axial rotation of the wheel and support the tire-wheel assembly. A steel platen 26-in. square and 6-in. thick, suspended from four 0.5-in-diameter vertical cables 6.5-ft long is used to apply the vertical load to the tire. Each cable is suspended from a load cell (with a span of 0 to 50 000 lb and a loading accuracy of ±30 lb) connected to a screw jack that is mechanically driven by an electric motor. The four cables move simultaneously and displace the platen in the vertical direction to load or unload the tire. A gritty film is applied to the platen surface to reduce tire footprint slippage. A two-degree-of-freedom analysis of the platen motion that confirms that the cable-suspended system has no significant coupling between the pitching and translating motions is given in reference 30.

Quasi-static lateral loading and quasi-static fore-and-aft loading of the tire were attained by displacing the platen in the lateral or fore-and-aft direction by means of a hydraulic cylinder after a vertical load was applied. Lateral (side) forces were measured by a load cell (with a span of 0 to 50 000 lb and a loading accuracy of ±30 lb) connected in series with the hydraulic cylinder. A similar instrumentation configuration was used to measure fore-and-aft (braking) forces and is shown in figure 6. Vertical, lateral, and fore-and-aft displacements of the platen were measured by displacement transducers (with a span of 0 to 5.5 in. and a measurement accuracy of ±0.02 in.). Platen displacements were considered to be equal to tire footprint displacements. Axial rotational movements between the wheel and the adapter plates were measured with a direct current displacement transducer (DCDT). An extensiometer fabricated from a 3-in. copper beryllium strain-gauge arch capable of measuring small displacements was used to measure tire-wheel slippage, which sometimes occurred during testing of the radial-belted tire. This tire-wheel slippage may be caused by the difference between the radial-belted and bias-ply tire

bead zone, which along with lower structural stiffness characteristics of the radial-belted tire, could induce different contact pressures and stress fields in the wheel (ref. 36).

For the quasi-static combined vertical-lateral and combined vertical fore-and-aft tests, vertical load was applied to the tire and maintained at the tire-rated load of 25 000 lb. A side load was gradually applied up to the maximum load of 3000 lb and then reduced to zero. This side force was restricted to a level at which no tire footprint slippage was discernible and which corresponded to 12 percent of the vertical load. This loading process was repeated in the opposite direction and resulted in four cycles that formed a hysteresis loop. The data acquisition system was manually triggered at side-load increments of 250 lb. Data from the various sensors were fed into a computer and afterwards saved for further reduction and analysis. Similar loading and data reduction procedures were used for the combined vertical fore-and-aft tests.

For the free-vibration tests, a quick-release mechanism in series with a hydraulic cylinder is connected to the platen by a 0.24-in-diameter steel cable. This hydraulic cylinder is used to apply a lateral or fore-and-aft load to the tire and then the load is released, causing the tire wheel-platen assembly to vibrate. A displacement transducer is used to determine lateral and fore-and-aft footprint deflections, and a 25*g* accelerometer is used to measure tire-platen accelerations. Figure 7 shows this test fixture in the fore-and-aft free-vibration test configuration.

Dynamic tire characteristics were obtained from simple, single degree-of-freedom free-vibration tests. These tests were conducted through a vertical load range of 5000 to 25 000 lb in 5000-lb increments. The specified vertical load was applied and then a side or braking force was applied up to 3000 lb. A quick-release mechanism was activated, causing the tire wheel-platen assembly to freely vibrate. The instrumentation output data were recorded by a computer that was manually triggered just prior to the activation of the quick-release mechanism. The data were saved for further reduction and analysis.

Test apparatus no. 2 was also used to obtain tire footprint geometrical properties for each tire design. The footprints were obtained from static vertical loads ranging from 5000 to 25 000 lb in 5000-lb increments. The process to obtain the footprints involved coating the tire tread with ink or chalk and applying the desired vertical load to the tire on a cardboard sheet located between the tire and the platen. Geometrical properties were obtained with a computerized planimeter from the resulting footprint silhouettes.

Test Apparatus No. 3

Mass moment-of-inertia properties of the tires tested were measured by using the torsional pendulum shown in figure 8. The torsional pendulum used for these tests consists of two 24-in-diameter circular plates bolted together and suspended in parallel by three equally tensioned, 17-ft wire cables that are attached to an overhead support. An index in 5° increments up to ±20° is scribed on the plate. A pointer is aligned with the index at 0° as a reference mark.

The tare moment of inertia of the two plates was initially determined by rotating the plate assembly through a predetermined angle and releasing it. The plate assembly was rotated 3 times at approximately 10°, 7.5°, 5°, and 2.5° for 20 oscillations each, and the time was recorded with a standard stopwatch. Similar tests were conducted with the inflated tire, with the wheel assembly, and with the rotors suspended between the plates. The weights of the plates and the tire-wheel assembly were recorded.

Damping Models

To optimize the performance of landing gear, designers and engineers must analyze all landing-gear parts that play key roles. The tires are one key element. Understanding the dynamic behavior of aircraft tires is important for the optimum design and operation of the aircraft and its landing gear. Antiskid braking systems are affected by the tire’s elastic responses; cross-wind landings are affected by the tire’s lateral dynamic behavior; shimmy is influenced by the tire's torsional behavior. Analysis of the damping properties and how different types of damping can influence tire performance is important in correcting these potential problems.

This section reviews three simple damping models: viscous, structural, and Coulomb friction. These models were chosen because of their simplicity and because a global view of damping was desired. The models only provide some insight into the damping mechanisms that might be present during quasi-static and dynamic tire testing and are not presented as accurate models for characterizing aircraft tire damping. (See refs. 30 and 37–40.)

Viscous Damping

In the study of vibrations, the viscous damper (dashpot) is the most common type of energy-dissipating element and is defined as a resistive force exerted on a body moving in a viscous fluid. An example of a viscous damper in aircraft is the landing-gear shock absorber.

In developing the viscous damping equations, it was assumed that the tire is represented by a linear elastic spring in parallel with a damping element to obtain an

approximation of its damping behavior. To more realistically represent the tire, a viscoelastic model should be used with an additional spring placed in series with the damper. However, this model is less attractive analytically since the in-series spring and damper elements have frequency-dependent parameters (ref. 34).

The viscous damping factor ζ, which is the ratio of the actual damping present in the system to the critical damping constant for the system, is given by

$$\zeta = \frac{c}{C_c} = \frac{c}{2m\omega_n} \tag{1}$$

The tire wheel-platen system was of the damped free-vibration type in which energy was dissipated from the system. In this study, the response of the free-vibration system was assumed to be underdamped so that $0 < \zeta < 1$ and $c < 2m\omega_n$:

$$x(t) = Ae^{-\zeta\omega_n t}\cos(\omega_d t - \phi) \tag{2}$$

Equation (2) can be interpreted as oscillatory motion with constant frequency ω_d and phase angle ϕ but with exponentially decaying amplitude $Ae^{-\zeta\omega_n t}$ as seen in figure 9.

The rate at which the maximum amplitude decays is expressed in terms of the natural log of an amplitude ratio that is known as the log decrement denoted by δ:

$$\delta = \ln\left(\frac{x_1}{x_2}\right) = \zeta\omega_n\tau = \frac{2\pi\zeta}{\sqrt{(1-\zeta^2)}} \tag{3}$$

$$\zeta = \frac{\delta}{\sqrt{[(2\pi)^2 + \delta^2]}} \tag{4}$$

$$\zeta \cong \frac{\delta}{2\pi} \tag{5}$$

Table 2 gives a summary of the viscous damping parameters.

Structural Damping

Solid materials exhibit structural or hysteretic damping. This type of damping is caused by internal friction in the material as internal planes slip or slide during deformation and is commonly seen as a hysteresis loop in which a phase lag between force and deflection exists. The area enclosed in the hysteresis loop represents the energy loss per loading cycle and can be written as

$$\Delta E_{\text{cyc}} = \int_{\text{cyc}} F\,dx = \int_0^{2\pi/\omega} F\dot{x}\,dt \tag{6}$$

Although structural damping is the most common type of damping, in free-vibration studies structural damping becomes indistinguishable from viscous damping and is difficult to treat analytically since it is defined in terms of energy loss and a nonlinear function of displacement. It is more convenient to express structural damping in terms of an equivalent viscous damping factor.

For the free-vibration case, the damping force is defined by the damping constant and the first derivative of displacement:

$$F = c\dot{x} = c\omega X\cos(\omega t + \phi) \tag{7}$$

Substituting F from equation (7) into equation (6) yields

$$\Delta E_{\text{cyc}} = c\omega^2 X^2 \int_0^{2\pi/\omega} \left\{\frac{1}{2}[1 + \cos 2(\omega t + \phi)]\right\} dt \tag{8}$$

$$\Delta E_{\text{cyc}} = c\omega^2 X^2 \left[\left(\frac{t}{2}\right) + \left(\frac{1}{\omega}\right)\sin\omega t\cos\phi\right]_0^{2\pi/\omega} \tag{9}$$

$$\Delta E_{\text{cyc}} = c\omega\pi X^2 \tag{10}$$

Systems possessing structural damping that are subjected to harmonic excitation may be treated as if they were subjected to equivalent viscous damping:

$$C_{\text{eq}} = \frac{\beta k}{\omega} \tag{11}$$

The energy dissipated per cycle for structural damping is independent of the frequency and proportional to the stiffness of the material and the square of the displacement amplitude. Substituting C_{eq} from equation (11) for c in equation (10) yields

$$\Delta E_{\text{cyc}} = \pi\beta k X^2 \tag{12}$$

Then β can be determined by using the log decrement method for a free-vibration system as was done in the viscous damping case. The energy equation for the half cycle between t_1 and t_2 is

$$\frac{kX_1^2}{2} - \frac{\pi\beta kX_1^2}{4} - \frac{\pi\beta kX_{1.5}^2}{4} = \frac{kX_{1.5}^2}{2} \tag{13}$$

$$\frac{kX_1^2}{2} - \frac{\pi\beta kX_1^2}{4} = \frac{kX_{1.5}^2}{2} + \frac{\pi\beta kX_{1.5}^2}{4} \tag{14}$$

$$\frac{kX_1^2}{2}\left(1 - \frac{\pi\beta}{2}\right) = \frac{kX_{1.5}^2}{2}\left(1 + \frac{\pi\beta}{2}\right) \tag{15}$$

The energy loss in a half-cycle is assumed to be proportional to that of a full cycle. Simplifying equation (15) yields

$$\frac{X_1^2}{X_{1.5}^2} = \frac{1+\frac{\pi\beta}{2}}{1-\frac{\pi\beta}{2}} \tag{16}$$

Looking at the next half-cycle,

$$\frac{X_{1.5}^2}{X_2^2} = \frac{1+\frac{\pi\beta}{2}}{1-\frac{\pi\beta}{2}} \tag{17}$$

Combining equations (16) and (17) gives a ratio of two successive amplitudes:

$$\frac{X_1}{X_2} = \frac{1+\frac{\pi\beta}{2}}{1-\frac{\pi\beta}{2}} \tag{18}$$

where β is very small for most materials and thus can be written as

$$\frac{X_1}{X_2} \cong 1+\pi\beta \tag{19}$$

The log decrement is thus

$$\delta = \ln\left(\frac{X_1}{X_2}\right) = \ln(1+\pi\beta) \cong \pi\beta \tag{20}$$

$$\beta = \frac{\delta}{\pi} \tag{21}$$

In the case of a quasi-static test, structural damping can be mathematically written in terms of the viscous damping factor ζ by the complex stiffness equation

$$F = (1+i2\zeta)kx \tag{22}$$

where

F external force on system
ζ viscous damping factor
k total spring rate
x complex displacement

The complex sinusoidal force is given by the following:

$$F = F_0 e^{i\omega t} \tag{23}$$

where

F_0 initial applied-force magnitude
ω circular forcing frequency

Substituting F from equation (22) into equation (23) yields

$$F_0 e^{i\omega t} = (1+i2\zeta)kx \tag{24}$$

Simplifying equation (24) and solving for x,

$$x = \frac{F_0/k}{(1+i2\zeta)} e^{i\omega t} \tag{25}$$

$$x = \frac{F_0/k}{(1+4\zeta^2)}(1-i2\zeta)e^{i\omega t} \tag{26}$$

Converting $(1-i2\zeta)$ to polar notation by using figure 10 and the following relationship of θ to ζ

$$\tan^{-1}\left(\frac{-2\zeta}{1}\right) = \theta \tag{27}$$

yields, for small angles,

$$\theta = -2\zeta \tag{28}$$

$$(1-i2\zeta) = re^{i\theta} \tag{29}$$

$$r = \sqrt{1+4\zeta^2} \tag{30}$$

Substituting θ from equation (28) and r from equation (30) into equation (29),

$$(1-i2\zeta) = \sqrt{(1+4\zeta^2)}\ e^{i(-2\zeta)} \tag{31}$$

Substituting $(1-i2\zeta)$ from equation (31) into equation (26) yields

$$x = \frac{F_0/k}{\sqrt{(1+4\zeta^2)}} e^{i(\omega t-2\zeta)} \tag{32}$$

A plot of displacement with respect to applied force yields a hysteresis loop whose width increases with ζ. The relationship of the width of the hysteresis loop to the damping factor can be derived by using the real part of the complex applied force F and displacement x:

$$e^{i\omega t} = \cos\omega t \tag{33}$$

$$e^{i(\omega t-2\zeta)} = \cos(\omega t-2\zeta) - i\sin(\omega t-2\zeta) \tag{34}$$

Substituting $e^{i\omega t}$ from equation (33) into equation (23) gives

$$F = F_0\cos\omega t \tag{35}$$

Substituting $e^{i(\omega t - 2\zeta)}$ from equation (34) into equation (32) yields

$$x = \frac{F_0/k}{\sqrt{1 + 4\zeta^2}} \cos(\omega t - 2\zeta) \tag{36}$$

For $x = 0$, $\cos(\omega t - 2\zeta) = 0$. Therefore,

$$\omega t = \frac{\pi}{2} + 2\zeta, \frac{3\pi}{2} + 2\zeta, \ldots \tag{37}$$

From equation (35) the applied force at zero displacement can be defined for small damping by the following:

$$F_{x=0} = F_0 \cos\left(\frac{\pi}{2} + 2\zeta\right) \tag{38}$$

For small angles,

$$F_{x=0} = 2\zeta F_0 \tag{39}$$

and

$$\zeta = \frac{1}{2}\left(\frac{F_{x=0}}{F_{\max}}\right) \tag{40}$$

Equation (40) represents structural damping in terms of viscous damping, and the static damping factor is a function of the load values at zero displacement and at maximum displacement (depicted graphically in figure 11). Table 3 presents the structural damping parameters.

Coulomb Friction

Coulomb (dry friction) damping occurs when bodies slide on dry surfaces. Motion begins when there is a force acting upon the body that overcomes the friction that resists this motion. This dry friction force is parallel to the surface and proportional to the normal force to the surface:

$$F_d = \mu_k W \tag{41}$$

The decay is linear with time (fig. 12), and the motion stops when the displacement is not sufficient for the spring's restoring force to overcome static friction. Decay occurs at the end of the half cycle when the amplitude is smaller than $2f_d$:

$$(x_1 - x_{-1}) = \frac{2F_d}{k} = 2f_d \tag{42}$$

Repeating for the next half-cycle,

$$(x_1 - x_2) = \frac{4F_d}{k} = 4f_d \tag{43}$$

For the static test case, the determination of the Coulomb friction parameters is shown in figure 13, where the damping force is defined as

$$F_d = \mu W \tag{44}$$

From figure 13,

$$A = 2F_d = 2\mu W \tag{45}$$

Stiffness properties can be determined from the spring rate

$$k = \frac{B}{C} = \frac{2F_d}{2X} \tag{46}$$

Table 4 presents the Coulomb friction parameters.

Data Reduction and Analysis

Basic data reduction techniques used in this investigation that enabled the comparison and analysis of static and dynamic (free-vibration) data are presented in the following sections.

Spring Rate

Spring-rate (stiffness) values give an indication of the types of vertical perturbations, elastic responses, and lateral stability characteristics of an aircraft tire. Spring-rate values for each tire design were computed from experimental data for both the quasi-static and free-vibration lateral and the fore-and-aft load tests, as well as for the quasi-static vertical-load tests.

Quasi-static tests. The quasi-static vertical, lateral, and fore-and-aft spring rates were determined by measuring the slope at specific points of load application and initial load relief that are defined by the vertical, lateral, and fore-and-aft load-deflection curves. The upper limit of the initial load-relief curve was not considered because of the uncertain value of the turnaround point as a result of the mechanical system limitation. The following steps were used for calculating the slopes of the load application and initial load-relief curves. The slopes are represented by the solid lines that are tangent to the curves, as shown in figure 14.

1. A second-degree polynomial curve fit was chosen for each loading cycle, and a third-degree polynomial curve fit was chosen for each unloading cycle of the hysteresis loop.

2. The start and end points for calculating the slope on the loading and unloading curves were selected by using a computerized digitizer.

3. The slope was calculated at discrete points along the loading or unloading curve within the bounds of the selected start and stop points.

The method described previously is normally used to obtain the tire spring rate from a quasi-static load-deflection curve. However, in order to compare the quasi-static and dynamic spring-rate values for the lateral and fore-and-aft tests, a technique that considers the effect of cable interaction was used. The slope of the quasi-static force-displacement hysteresis-loop axis (the dashed line connecting the loop extremes, as shown in fig. 14) defines the total stiffness applied to the platen k_p. The tire spring rate k_t is then determined by subtracting the cable interaction stiffness k_c from the platen spring rate. (See ref. 30.)

$$k_c = \frac{F}{l_c} \tag{47}$$

$$k_t = k_p - k_c \tag{48}$$

where

F load applied to the system, lb
l_c free swing cable length = 6.5 ft
k_t tire spring rate, lb/in.
k_p platen spring rate, lb/in.
k_c spring rate from cable interaction, lb/in.

Dynamic tests. For the lateral and fore-and-aft free-vibration tests, the tire spring rate is also a function of the platen spring rate minus the spring rate from cable interaction. Since the frequency is a function of the platen spring rate and the mass of the platen m_p, the spring rate k_p may be calculated as follows (ref. 30):

$$f = \frac{1}{2\pi}\sqrt{\frac{k}{m}} \tag{49}$$

$$\frac{k}{m} = (2\pi f)^2 = \left(\frac{2\pi}{\tau}\right)^2 \tag{50}$$

where

f frequency, Hz
$\frac{k}{m}$ frequency parameter $= \left(\frac{2\pi}{\tau}\right)^2$
τ period of oscillation, sec

The period is measured from the displacement time-history plots from which the frequency parameter is determined. The total spring rate acting on the platen is then

$$k_p = (2\pi f)^2 m_p \tag{51}$$

$$k_p = \frac{k}{m}\left(\frac{w_p}{\alpha}\right) \tag{52}$$

where

w_p platen weight = 1182 lb
α acceleration = 32.2 ft/sec^2

As in the quasi-static case, the spring rate, caused by cable interaction k_c must be subtracted from k_p, and the tire spring rate then becomes

$$k_t = k_p - k_c \tag{53}$$

Damping Factor

Damping factors were determined for both the quasi-static and dynamic lateral tests and also for the fore-and-aft tests that were conducted. These damping factors gave a first approximation of the damping type in the system and whether one tire type exhibited more damping than the other.

In this investigation, viscous and structural damping were determined based on system response characteristics. Coulomb friction, however, was not applicable to the system because the limited loads achieved in the lateral and fore-and-aft directions did not allow for large-scale (measurable) tire footprint slippage. If these tests were repeated at higher lateral and fore-and-aft loads, Coulomb friction might occur.

Quasi-static tests. For the quasi-static tests, the structural damping factor written in terms of the viscous damping factor ζ is determined from the lateral and fore-and-aft load values at zero and maximum tire deflections (fig. 11).

$$\zeta = \frac{1}{2}\left(\frac{F_{x=0}}{F_{\max}}\right) \tag{54}$$

where

$F_{x=0}$ load at zero deflection
$F_{\max}$ load at maximum deflection

Dynamic tests. For the dynamic tests, the viscous damping factor ζ is determined from the logarithmic

decrement of the decaying displacement amplitude of a displacement time-history plot

$$\zeta = \frac{1}{2\pi}\ln\left(\frac{X_1}{X_2}\right) \tag{55}$$

However, in these tests it was difficult to determine the logarithmic decrement directly from the time-history plots because of the drifting equilibrium level (X-axis). A more accurate viscous damping factor can be determined by computing a double amplitude from the difference between the spline-fitted displacement envelope that passes through the displacement extremes, as shown in figure 9. The logarithmic decrement δ and viscous damping factor ζ can then be expressed as follows:

$$\delta = \ln\left(\frac{2X_1}{2X_2}\right) \tag{56}$$

$$\zeta = \frac{\delta}{2\pi} \tag{57}$$

In the free-vibration case, the structural damping factor β can be written in terms of the viscous damping factor ζ.

$$\beta = 2\zeta \tag{58}$$

Energy Loss

The energy loss associated with hysteresis is another indicator of structural damping. For the quasi-static load-deflection curves, the energy loss is typically determined by the area enclosed in the hysteresis loop. To have a more precise comparison between the quasi-static and dynamic tests, the energy loss per cycle is computed as a function of the structural damping factor, the tire spring rate, and the maximum displacement amplitude for both test conditions

$$\Delta E_{cyc} = \pi\beta k_t X^2 \tag{59}$$

where

β structural damping factor = 2ζ
k_t tire spring rate, lb/in.
X maximum displacement amplitude, in.

Footprint Geometry

Footprint geometrical properties were determined from the net footprint area that was calculated from the following equation:

$$A_{net} = A_{gross} - A_{grooves} \tag{60}$$

where

A_{gross} area of entire footprint, in^2
$A_{grooves}$ area of tread grooves, in^2

Moment of Inertia

The mass moment of inertia for each tire design and the tare inertia for the two pendulum plates were calculated using the following equation:

$$J = \frac{\tau^2 W R^2}{4\pi^2 L} \tag{61}$$

where

J mass moment of inertia, in-lb-sec^2
τ average period of system oscillation, sec
W weight of object being measured, lb
R radial distance from center of plate to support cables, in.
L length of support cables, 17 ft

The mass moment of inertia of the tire and rotating parts was calculated using the following equation:

$$J_{tire} = \frac{\tau^2 W R^2}{4\pi^2 L} - J_{plates} \tag{62}$$

Results and Discussions

Several characteristics of the radial-belted tire have delayed its acceptance into the aircraft industry. The key to its gaining acceptance lies in understanding the differences between bias-ply and radial-belted tires. The following sections review the results of the vertical, the combined vertical-lateral, and the combined vertical fore-and-aft tests and make observations of the similarities and differences between the F-4 radial-belted aircraft tire and its bias-ply counterpart.

Quasi-Static Pure Vertical Load Tests

Quasi-static (nonrolling) vertical load tests were completed with a bias-ply and a radial-belted F-4 aircraft tire. Results of these tests are presented in the form of vertical load-deflection curves, vertical spring rate, and energy loss associated with hysteresis.

Load deflection. As each tire came into contact with the frictionless table, vertical load was applied until the desired load of 25 000 lb was reached. The applied load was then reduced to zero. The resulting load-deflection curve, or hysteresis loop, is indicative of tire vertical-loading behavior and provides information which defines the tire vertical spring rate and energy loss. Four load-deflection curves were generated for each tire at four different tire peripheral positions.

Figure 15 shows typical vertical load-deflection curves for the bias-ply and radial-belted tires: the lower bound of tire vertical stiffness is represented by the load-application curve, and the upper bound of tire vertical stiffness is represented by the initial load-relief curve. For the bias-ply tire, the data show that the vertical deflection is nonlinear at the initial load application but that it is linear over the remaining load-application range to the maximum load of 25000 lb. Analogous load-deflection characteristics apply to the load relief range. The loading-unloading process shows some hysteresis as a result of energy loss during this process. The maximum tire vertical displacement is 2.48 in.

For the radial-belted tire, the load deflection is nonlinear during the entire load application and the load relief cycles. The maximum tire vertical displacement is 2.53 in., which is 2 percent higher than that of the bias-ply tire.

The vertical load-deflection characteristics of radial-belted and bias-ply tires are of interest to strut designers. In general, the load-deflection characteristics are similar for the two tire designs tested and suggest that there should be no impact on strut valving and on the loads transmitted to the airframe for aircraft equipped with this radial-belted tire (ref. 6).

Spring rate. In order to cover the range of stiffness values that the tire would experience as a result of vertical perturbations during aircraft taxi, takeoff, and landing maneuvers, vertical stiffness data are presented in terms of tire spring rate (fig. 16). The lower bound of tire vertical stiffness for the bias-ply tire is represented by the load-application curve denoted by the square symbols, and the upper bound of vertical stiffness is represented by the load-relief curve denoted by the triangular symbols. Vertical spring-rate values were obtained by measuring the instantaneous slope along the vertical load-deflection curve. A regression analysis technique was used to fit a curve through the spring-rate data. At initial load application, the spring rate of the bias-ply tire increases linearly from 7121 lb/in. to 11 515 lb/in. and remains constant at this higher value for the remainder of the load application process. A maximum spring rate of 14 432 lb/in. is observed at load relief, which becomes nonlinear as the load decreases to 11 515 lb/in.

Vertical spring-rate values for the radial-belted tire are also shown in figure 16; the lower bound of tire vertical stiffness is represented by the load-application curve denoted by the diamond symbols, and the upper bound of vertical stiffness is represented by the load-relief curve denoted by the circular symbols. During load application, the tire spring rate is nonlinear and increases from 7170 lb/in. to 12 340 lb/in. The maximum spring rate for the radial-belted tire is 14 113 lb/in. at initial load relief and continues to decrease nonlinearly.

In figure 16, it can be observed that the vertical stiffness characteristics of the bias-ply and radial-belted tires are similar. One implication of this similarity is that the landing dynamics characteristics of an aircraft equipped with this radial-belted tire would be similar to an aircraft equipped with standard bias-ply tires.

Energy loss. Energy loss associated with hysteresis during the loading and unloading period is represented by the enclosed area of the load-deflection curve (fig. 15) and was measured using a computerized planimeter. This hysteresis loop arises largely as a consequence of the structural or hysteretic damping forces that oppose the tire deformation. The average energy loss is 2819 in-lb for the bias-ply tire and 2547 in-lb for the radial-belted tire under vertical-loading conditions.

The lower energy loss for the radial-belted tire suggests that there is less heat generated in the radial-belted tire during tire cyclic deformation; therefore, it should be a cooler operating tire. This suggested heat reduction may be a result of the tire construction, which produces lower internal shear stress and thus energy loss. The heat reduction could lead to improved tire durability and allow for shorter aircraft turnaround times (ref. 8).

Quasi-Static Combined Vertical-Lateral Load Tests

Quasi-static combined vertical-lateral load tests were conducted to determine the stiffness and damping characteristics of the two tire designs tested. These results are represented by load-deflection curves and spring-rate curves that are analyzed in the following sections.

Load deflection. An initial vertical load of 25 000 lb was applied to the tire, which was then subjected to a load of 3000 lb perpendicular to the wheel plane. Five individual curves (load application and load relief) were generated to obtain a complete hysteresis loop. Lateral (side) force and tire footprint displacement data were recorded at 250-lb side-load increments. Four load-deflection curves (hysteresis loops), each one corresponding to a different location 90° around the periphery of the tire, were developed. Typical load-deflection curves for the bias-ply and the radial-belted tires are shown in figure 17. Based on observed nonlinear trends, a second degree polynomial was chosen to curve fit the data points obtained during load application, and a third degree polynomial was chosen for the load relief data.

Results shown in figure 17 represent load-deflection characteristics of the bias-ply and radial-belted tires and demonstrate the hysteretic nature of the loading and

unloading cycles. A maximum deflection of 0.38 in. was obtained for the bias-ply tire under a 3000-lb side force. Under combined vertical-lateral loading conditions, the bias-ply tire exhibits linear characteristics during the entire load application cycle and nonlinear characteristics during initial load relief.

Similar lateral load-deflection characteristics were obtained for the radial-belted tire for both the loading and unloading cycles. The maximum lateral displacement was 0.52, which is a 37-percent increase in tire footprint displacement compared with its bias-ply tire counterpart. This increase in footprint displacement is a consequence of the radial-belted tire construction.

Spring rate. Lateral spring-rate values were obtained by evaluating the instantaneous slope along the loading and unloading curves. Lateral spring-rate values are plotted as a function of lateral displacements for all four peripheral tire positions for both the bias-ply and the radial-belted designs (fig. 18). Bias-ply tire spring-rate values decrease slightly from 7311 lb/in. to 7200 lb/in. during the load application process represented by the square symbols. During the initial load-relief process, spring-rate values, denoted by the triangular symbols, decrease from a maximum value of 10622 lb/in. to 7600 lb/in.

The radial-belted tire has slightly decreasing spring-rate values (symbolized by diamonds) from 5624 lb/in. to 5602 lb/in. during the load application cycle, as shown in figure 18. The maximum spring rate (represented by circles) of 8098 lb/in. is noted at initial load relief decreasing to 6098 lb/in.

Lateral stiffness characteristics of the tires are directly related to cornering and yaw response and are thus important to shimmy analysis as well as to the landing dynamics in a crosswind landing. The radial-belted tire's stiffness values are on average 24 percent lower than the comparable bias-ply tire. This reduction in lateral stiffness may indicate an increase in the incidence of landing-gear shimmy when this radial-belted tire replaces its bias-ply counterpart. Landing dynamics in a crosswind with this radial-belted tire may be affected as well.

Damping factor. The quasi-static structural damping factors, in terms of viscous damping, are determined from the maximum and minimum lateral load at zero displacement on the load-deflection curve (fig. 17). The computed static damping factors are 0.042 and 0.038 for the bias-ply and the radial-belted tires, respectively. The structural damping for the radial-belted tire is within 10 percent of that for the bias-ply tire, indicating that structural damping is similar for the two tires tested under quasi-static lateral loading conditions.

Energy loss. The area enclosed in the lateral load-deflection curves for the bias-ply and radial-belted tires is a measurement of the energy loss as a result of hysteresis (fig. 17). The average energy loss is 289 in-lb for the bias-ply tire and 300 in-lb for the radial-belted tire. The energy loss because of hysteresis during the lateral loading and unloading cycles is similar for the two tires that were tested, and thus the structural damping properties of the tires are similar under the given loading conditions.

Quasi-Static Combined Vertical Fore-and-Aft Load Tests

Quasi-static combined vertical fore-and-aft load tests were conducted to determine the fore-and-aft stiffness and damping characteristics from the resulting load-deflection curves. Results from these tests are given in the following sections.

Load deflection. Load deflection tests involved applying a maximum vertical load of 25000 lb and a fore-and-aft load of 3000 lb to the tire. Braking force and tire footprint displacement data were recorded at 250-lb load increments. Four load-deflection curves were generated, each one corresponding to a different location 90° around the periphery of the tire. A second degree polynomial was chosen to curve fit the data points obtained during load application in the fore or aft directions, and a third degree polynomial was chosen for load relief data. Typical plots showing data with curve fits for each tire tested are shown in figure 19.

Results shown in figure 19 for the bias-ply tire represent fore-and-aft load-deflection characteristics that are corrected for wheel adapter plate slippage and demonstrate the hysteretic nature of the loading and unloading process. A maximum deflection of 0.19 in. was obtained for the bias-ply tire under a 3000-lb fore-and-aft (braking) force. The tire exhibits linear characteristics during the entire load application cycle and nonlinear characteristics during initial load relief.

Similar load-deflection characteristics were obtained for the radial-belted tire that were corrected for tire-wheel slippage as well as for wheel adapter plate slippage (ref. 12). The radial-belted tire exhibits characteristics similar to the bias-ply tire during both load application and load relief. The maximum fore-and-aft displacement is 0.27 in. This 42-percent difference in tire deflection between the bias-ply and the radial-belted tires can be attributed to the difference in the elastic properties of the tire designs (ref. 5).

Spring rate. Fore-and-aft spring-rate values were obtained by evaluating the instantaneous slope of each loading and unloading interval along the load-deflection curves. Fore-and-aft spring-rate values are plotted as a function of fore-and-aft footprint displacements for both tire designs in figure 20. Bias-ply tire spring-rate values linearly decrease from 15140 lb/in. to 12944 lb/in. during the load-application process and are represented by the square symbols. During initial load relief, spring-rate values (triangular symbols) decrease from a maximum value of 26495 lb/in. to a minimum value of 18131 lb/in.

The radial-belted tire has linear spring-rate trends during load application (diamond symbols) where the spring rate decreases by 1.6 percent from 11343 lb/in. to 11157 lb/in. The maximum spring rate of 15833 lb/in. is at initial load relief and decreases to 12870 lb/in. These values are represented by the circular symbols.

The stiffness values for the radial-belted tire were 14 to 40 percent lower than the stiffness values for the bias-ply tire. The lower fore-and-aft stiffness values of the radial-belted tire may introduce a lag between the braking effort and the ground reaction that could affect the dynamics of antiskid braking systems used with this radial-belted tire but that are "tuned" for bias-ply tires (ref. 5).

Damping factor. Structural damping factors for quasi-static tests were determined from the fore-and-aft maximum and minimum load at zero displacement on the load-deflection curves (fig. 19). The computed quasi-static structural damping factors are 0.068 and 0.044 for the bias-ply and the radial-belted tires, respectively. These data indicate that there is 35 percent more damping occurring in the bias-ply tire than in the radial-belted tire during quasi-static fore-and-aft tests.

Energy loss. The static fore-and-aft energy loss associated with hysteresis for the bias-ply and the radial-belted tires is represented by the area enclosed in the fore-and-aft load-deflection curves (fig. 19). The average energy loss is 229 in-lb for the bias-ply tire and 169 in-lb for the radial-belted tire, which is 26 percent lower than the bias-ply tire. These results are in agreement with the values determined for the structural damping factor and suggest that the radial-belted tire should operate at lower temperatures than the comparable bias-ply tire. The results also suggest the possibility of less wear for the radial-belted tire during cyclic braking operations.

Free-Vibration Combined Vertical-Lateral Load Tests

Results are presented in this section from the free-vibration, combined vertical-lateral load tests for each tire design. Lateral spring rate, damping factor, and energy loss values were obtained from the displacement time-history plots.

Time-history plots. Ten displacement time-history plots and 10 acceleration time-history plots were generated for each tire type tested at two different tire peripheral positions. A specified vertical load was applied to the tire, and then a side load of 3000 lb was applied and released, resulting in the displacement and acceleration response of the platen to a free-vibration test, as shown in figure 21. Final reference displacement levels are shown along with the displacement and acceleration envelopes. This shift in equilibrium level was attributed to tire creep (ref. 30). Tests were conducted at vertical loads of 5000 lb up to 25000 lb in 5000-lb increments.

From the bias-ply tire time-history plots for vertical loads of 5000 lb to 25000 lb, the system was underdamped, exponentially decaying, and had a decreasing frequency from 8 to 6 Hz as the vertical load decreased, thus indicating that the period of oscillation is sensitive to changes in vertical load. As shown in figure 21 at 25000-lb vertical load, the maximum bias-ply tire displacement amplitude is 0.32 in. and the maximum acceleration is 2.14*g*.

The time-history plots for the radial-belted tire at 25000-lb vertical load are also shown in figure 21. The maximum tire displacement is 0.37 in. and maximum acceleration is 2.12*g*. The frequency of oscillation decreases from 8 Hz to 6 Hz as the vertical load decreases from 25000 lb to 5000 lb.

During the lateral free-vibration tests, the bias-ply and radial-belted tire had similar acceleration and frequency characteristics. However, the radial-belted tire footprint deflection, which was attributed to tire construction, was 16 percent greater than that of the bias-ply tire.

Spring rate. The lateral spring-rate values were determined from the frequency of vibration, the weight of the platen, and the frequency parameter for each tire design and are plotted as a function of the vertical load in figure 22. In general, the spring-rate values increase as vertical load increases for each tire design. Both tires exhibit nonlinear spring-rate characteristics. The bias-ply tire has higher spring-rate values that range from 5225 lb/in. to 7585 lb/in. for the same vertical loads as the radial-belted tire, whose tire spring-rate values range from 4757 lb/in. to 6676 lb/in. The spring-rate values of the bias-ply tire are 9 to 12 percent higher than those of the radial-belted tire and were expected to be because of the bias-ply tire's stiffer sidewall construction.

Tire lateral stiffness measurements are important properties in the dynamic analysis of aircraft wheel shimmy. The lower stiffness values of the radial-belted tire imply that tire wheel shimmy conditions may exist when this tire is used.

Damping factor. Lateral viscous damping factors were determined from the tire displacement amplitudes of the time-history plots by using the log decrement method. The viscous damping factor, as a function of vertical load for each tire, is shown in figure 23. As the vertical load increases, the damping factor decreases for both tire designs and thus is sensitive to the vertical load range that is applied during these free-vibration tests. The viscous damping factor values for both tire designs are lowest at 20000 lb of vertical load. The bias-ply tire shows higher viscous damping factor values that range from 0.088 to 0.047; the values of the radial-belted tire range from 0.07 to 0.031. Thus, viscous damping is greater in the bias-ply tire than in the radial-belted tire under these loading conditions.

In order to verify the calculation of the damping factor when the log decrement method is used, a semilog plot of displacement amplitude, as a function of the number of cycles, is shown in figure 24. The linear characteristics of both tires indicate that the log decrement method yields consistent results for the first four cycles of these tests.

The lateral structural damping factor in terms of viscous damping was determined from the tire displacement time-history plots. Bias-ply structural damping factor values range from 0.092 to 0.176, and the radial-belted tire values range from 0.062 to 0.14. The lower damping values of the radial-belted tire indicate that there is less structural damping under these loading conditions.

Energy loss. The dynamic lateral energy loss per cycle for each tire was calculated. The bias-ply tire has a calculated energy loss of 217 in-lb and the radial-belted tire has an energy loss per cycle of 175 in-lb, both at 25 000 lb of vertical load. Again, this result suggests that the radial-belted tire should be a cooler operating tire than the comparable bias-ply tire.

Free-Vibration Combined Vertical Fore-and-Aft Load Tests

Results from the free-vibration combined vertical fore-and-aft load tests for each tire design are presented in this section. Fore-and-aft spring rate, damping factor, and energy loss values were obtained from the displacement time-history plots generated from free-vibration tests.

Time-history plots. Ten displacement time-history plots and 10 acceleration time-history plots were generated for each tire at two different tire positions. A specified vertical load was applied to the tire and then a braking load of 3000 lb was applied and released. These tests were conducted at vertical loads from 5000 lb to 25000 lb in 5000-lb increments.

Typical displacement time-history and acceleration time-history plots for the bias-ply and the radial-belted tires at 25000-lb vertical load are shown in figure 25. The time-history plots show that the system is underdamped and is decaying exponentially. As in the dynamic lateral load tests, the displacement time-history plots exhibit a shift in the equilibrium level that is attributed to tire creep.

The maximum bias-ply tire displacement amplitude is 0.14 in. and the maximum acceleration is 2.0*g*. The frequency of vibration decreases from 13 Hz to 9 Hz as the vertical load decreases and indicates that the frequency is sensitive to variations in vertical load. The maximum radial-belted tire displacement is 0.16 in. and the maximum acceleration is 2.0*g*. The frequency of vibration decreases from 10 Hz to 7 Hz as the vertical load decreases.

Both tires have similar acceleration and frequency characteristics. The increase in radial-belted tire footprint displacement suggests a more elastic tire than the bias-ply tire under braking conditions. This increase in radial-belted tire elasticity could adversely affect the operation of an antiskid braking system designed for the less elastic bias-ply tire.

Spring rate. The fore-and-aft spring-rate values for each tire design are plotted as a function of the vertical load in figure 26. In general, the spring rate increases as vertical load increases for each tire design, and both tires show nonlinear spring-rate characteristics. The bias-ply tire has higher spring-rate values that range from 9201 lb/in. to 20610 lb/in. for the same vertical loads as the radial-belted tire. The radial-belted tire spring-rate values range from 5921 lb/in. to 11 025 lb/in. The spring-rate values of the radial-belted tire are 36 to 47 percent lower than those of the bias-ply tire, and these lower spring rate values may have an adverse affect on the antiskid braking system performance when this radial-belted tire is used.

Damping factor. Viscous damping factors were determined from the tire displacement amplitudes of the time-history plots. The damping factors, as a function of vertical load for each tire, are shown in figure 27. As the vertical load increases, the viscous damping factor

decreases for both tire designs. The bias-ply tire has higher viscous damping factors, ranging from 0.086 to 0.127, than those of the radial-belted tire, which range from 0.064 to 0.106. Structural damping in terms of viscous damping yields bias-ply tire values of 0.172 to 0.254 and radial-belted tire values of 0.128 and 0.212. Up to 26 percent more structural and viscous damping occurred in the bias-ply tire during these free-vibration tests.

Energy loss. The dynamic energy loss associated with hysteresis for each tire is calculated from the tire structural damping factor, the spring rate, and the maximum displacement amplitude. The bias-ply tire has a calculated energy loss of 204 in-lb; the radial-belted tire has an energy loss per cycle of 136 in-lb. These data suggest that the radial-belted tire generates less heat during the free-vibration tests, which should result in a lower operating temperature for this tire. Tires with lower operating temperatures tend to have less wear during normal braking operations.

Quasi-Static and Free-Vibration Lateral Load Data Comparison

A comparison of the quasi-static and free-vibration lateral load data for each tire design is presented in this section. Since the quasi-static tests were only conducted at the rated vertical load of 25000 lb, the comparison with the dynamic data was only at this vertical load. Table 5 presents the quasi-static and dynamic lateral load tire properties.

Spring rate. The bias-ply and the radial-belted tires exhibit very similar stiffness values in the quasi-static and dynamic data. The bias-ply quasi-static spring rate is 7214 lb/in. as compared with 5674 lb/in. for the radial-belted tire. The dynamic spring rates are 7585 lb/in. for the bias-ply tire and 6676 lb/in. for the radial-belted tire. The bias-ply tire has higher stiffness values than the radial-belted tire under both loading conditions because of its stiffer carcass. The increased stiffness values under free-vibration tests for the tires that were tested may be attributed to the viscoelastic nature of the tire material.

In the quasi-static tests, the stiffness of the radial-belted tire is 21 percent lower than that of the comparable bias-ply tire. However, the free-vibration tests give a more realistic view of what to expect under actual operating conditions, and in this case the radial-belted tire exhibits stiffness values that are 12 percent lower than those of the bias-ply tire. Although the radial-belted tire still exhibits lower lateral stiffness characteristics under free-vibration testing conditions, this 12-percent difference is encouraging, given the concerns in the aircraft tire industry about the lateral force capabilities of the radial-belted tire.

Damping factor. The calculated quasi-static structural damping factors in terms of viscous damping are 0.044 and 0.038 for the bias-ply and radial-belted tires, respectively. The viscous damping factor for the free-vibration test is 0.047 for the bias-ply tire and 0.031 for the radial-belted tire. The damping factor values are similar under both test conditions for both tire types.

Energy loss. The calculated quasi-static energy loss for the bias-ply and radial-belted tires are similar: 319 in-lb and 339 in-lb, respectively. For the free-vibration tests, the computed energy loss is 217 in-lb for the bias-ply tire and 175 in-lb for the radial-belted tire. The energy loss values in the free-vibration case were lower than those calculated under static testing conditions (32 percent for the bias-ply tire and 48 percent for the radial-belted tire). The quasi-static test conditions produced more tire hysteresis than the free-vibration test conditions produced.

Quasi-Static and Free-Vibration Fore-and-Aft Load Data Comparison

A comparison of the quasi-static and free-vibration fore-and-aft load data for each tire design is presented in this section. Since the quasi-static data were gathered only at the rated vertical load of 25000 lb, the comparison with the dynamic data was conducted only at this vertical load. Table 6 presents both quasi-static and dynamic fore-and-aft load data.

Spring rate. The quasi-static spring-rate values are 16145 lb/in. and 9394 lb/in. for the bias-ply and the radial-belted tires, respectively. The spring rates for the free-vibration tests are 20601 lb/in. and 11025 lb/in. for the bias-ply and the radial-belted tires, respectively. The results show that both tires are stiffer during fore-and-aft free-vibration tests than during quasi-static tests; the increased stiffness may be partly attributed to the viscoelastic nature of the tires.

Damping factor. The calculated quasi-static structural damping factors in terms of viscous damping are 0.055 and 0.036 for the bias-ply and the radial-belted tires, respectively. The viscous damping factor for the free-vibration tests is 0.086 for the bias-ply tire and 0.064 for the radial-belted tire. The quasi-static tests resulted in lower structural damping factors, in terms of viscous damping, than the free-vibration tests viscous damping factors. These data suggest that possibly some viscous damping, as well as the assumed structural damping, occurs under free-vibration testing conditions.

Energy loss. The calculated quasi-static energy loss for the bias-ply and the radial-belted tires is 222 in-lb and 128 in-lb, respectively. For the free-vibration tests, the computed energy loss is 204 in-lb for the bias-ply tire and 135 in-lb for the radial-belted tire. The bias-ply tire's calculated quasi-static energy loss is 9 percent higher than its dynamic energy loss. The calculated quasi-static energy loss for the radial-belted tire is 5 percent lower than its dynamic energy loss. These differences between the quasi-static and dynamic energy loss measurements for each tire are small and indicate that the tires have similar hysteretic characteristics under both testing conditions**.**

Footprint Geometrical Properties

Footprint geometrical properties help predict tire hydroplaning characteristics. Results from tire footprint measurements for each tire design are presented in this section.

Tire footprints were obtained for each tire under various vertical loads. Geometric parameters such as footprint area, length, and width were measured from the resulting footprint silhouettes. A plot of net footprint area as a function of vertical load is shown in figure 28. The bias-ply tire has a greater footprint area than the radial-belted tire for the same vertical loads. This larger footprint area is also evident in the tire footprint silhouettes that are shown in figure 29 and that were taken at a maximum rated load of 25000 lb. The bias-ply tire has a more rectangular footprint, and the radial-belted tire has a more oval footprint. At 245 psi, the predicted hydroplaning speed of the bias-ply tire is 141 knots; the predicted hydroplaning speed of the radial-belted tire at 310 psi is 159 knots (ref. 41). However, the increased hydroplaning speed for the radial-belted tire at the higher inflation pressure may not be realized because of adverse effects associated with the aspect ratio (height-to-width ratio of the tire footprint) of the nearly circular footprint of the radial-belted tire (ref. 42). In general, these tests suggest that the bias-ply tire may perform more favorably under wet runway conditions.

Moment-of-Inertia Properties

Inertia properties of tires help to define the tire's spin-up characteristics during touchdown. Moment-of-inertia tests were conducted for both tire designs and the results are presented.

The mass moment of inertia for each tire design and the tare inertia for the two pendulum plates were calculated. The moment of inertia is 4.35 in-lb-sec^2 for the plates, 31.5 in-lb-sec^2 for the bias-ply tire, and 27.7 in-lb-sec^2 for the radial-belted tire. The moment of inertia of the radial-belted tire is 12 percent lower than that of the bias-ply tire. This difference implies that the radial-belted tire would require slightly less energy to spin up during the landing touchdown than the bias-ply tire would. Less energy needed in the spin-up portion of a touchdown could mean reduced tread wear during high-speed landings.

Concluding Remarks

An investigation at the Langley Research Center was conducted to determine, evaluate, and compare certain quasi-static and dynamic mechanical properties of the U.S. Air Force F-4 military fighter 30×11.5-14.5/26PR bias-ply and radial-belted main gear tires that define their performance during taxi, takeoff, and landing operations and to define the suitability of the radial-belted tire as a replacement for the bias-ply aircraft tire. These properties were obtained from quasi-static vertical, lateral, and fore-and-aft load-deflection data; lateral and fore-and-aft free-vibration time-history plots; tire footprint measurements; and moment-of-inertia tests. Three damping models: viscous, structural, and Coulomb friction were presented that gave an insight into the type of damping that occurs under both quasi-static and free-vibration test conditions.

The results of this investigation indicate the following observations:

1. In general, the radial-belted tire has vertical load characteristics that are similar to those of the conventional bias-ply tire. However, significant differences are observed between the bias-ply and the radial-belted tires' lateral and fore-and-aft load characteristics.

2. Vertical load-deflection characteristics obtained for the radial-belted and the bias-ply tires for the given load range are similar. Under lateral and fore-and-aft load conditions, the radial-belted tire has greater footprint displacements. This radial-belted tire has a more circular footprint and less tread in contact with the surface than its bias-ply tire counterpart.

3. Vertical stiffness characteristics obtained for the radial-belted and bias-ply tires are similar for the given load range considered in this study. Radial-belted stiffness values are lower under quasi-static and dynamic lateral and fore-and-aft testing conditions. Test results indicate that both tire designs are stiffer during free-vibration tests than during quasi-static tests.

4. Energy loss associated with hysteresis of the radial-belted tire is less than that of the bias-ply tire under vertical and fore-and-aft quasi-static test conditions, as well as under lateral and fore-and-aft free-vibration test conditions. Damping characteristics are similar for both tires under quasi-static lateral loads.

Quasi-static tests resulted in lower damping at the rated vertical load of 25000 lb than the free-vibration tests had at that load. The radial-belted tire has lower moment of inertia values than the bias-ply tire.

The following conclusions are made from the above observations:

1. Similar vertical load stiffness characteristics between the two tire designs imply that there should be no impact on strut valving, on the loads transmitted to the airframe, and on the landing dynamics for aircraft equipped with this radial-belted tire under normal operating conditions.
2. Lateral and fore-and-aft stiffness properties of this radial-belted tire may result in an increase in tire shimmy and may affect the performance of an anti-skid braking system "tuned" for bias-ply tires. The increased overall stiffness properties of the two tire designs during free-vibration tests, compared with the quasi-static tests, may be attributed in part to the viscoelastic nature of the tires. Footprint geometrical properties of the radial-belted tire suggest that it might be more sensitive to hydroplaning conditions than its bias-ply tire counterpart.
3. The energy loss measured for the radial-belted tire suggests that lower operating temperatures during normal ground and braking operations may lead to improved tire durability. The lower temperatures of the radial-belted tire could allow for shorter aircraft turnaround time and less tread wear. Similar temperature profiles may occur during cornering maneuvers. A comparison of the higher damping factors under fore-and-aft free-vibration tests with quasi-static tests for both tire designs suggests that some viscous damping is present, as well as the assumed structural damping. Moment-of-inertia tests indicate that the radial-belted tire requires less energy to spin up during touchdown, and that less energy may result in reduced tread wear and reduced heating during high-speed landings.

NASA Langley Research Center
Hampton, VA 23681-0001
May 22, 1996

References

1. Currey, Norman S.: Aircraft Landing Gear Design—Principles and Practices. *AIAA*, 1988, p. 1
2. Birch, Stuart: Aircraft Tyres. *Aerosp. Eng.*, vol. 7, Sept. 1987, pp. 24–27.
3. Massey, Antoine: Radial-Belted Aircraft Tyres Take Off. *Aerosp. Design Eng.*, May 1992, pp. 223–226.
4. Smiley, Robert. F.; and Horne, Walter B.: *Mechanical Properties of Pneumatic Tires With Special Reference to Modern Aircraft Tires*. NASA TR R-64, 1960.
5. Tanner, John A.: *Fore-and-Aft Elastic Response Characteristics of 34×9.9, Type VII 14 Ply-Rating Aircraft Tires of Bias-Ply, Bias-Belted, and Radial-Belted Design*. NASA TN D-7449, 1974.
6. Alsobrook, C. B.: *Radial Aircraft Tires in Perspective.* SAE Paper 871869, Oct. 1987.
7. Cesar, J. P.; Musy, J.; and Olds, R.: Development of Radial Aircraft Tires. Michelin Paper Presented to *38th International Air Safety Seminar* (Boston, Massachusetts), Nov. 4–7, 1985.
8. Olds, R.: *Development of Radial Aircraft Tires.* SAE Paper 871870, Oct. 1987.
9. Lewis, W. M.: *AV-8B Radial Ply Construction Aircraft Tire Evaluation*. NATC-SA-6R-87, Naval Air Test Center, (Patuxent River, Maryland), Mar. 1987.
10. Dodge, R. N.; Orne, David; and Clark, S. K.: *Fore-and-Aft Stiffness Characteristics of Pneumatic Tires*. NASA CR-900, Oct. 1967.
11. Davis, Pamela A.; and Lopez, Mercedes C.: *Static Mechanical Properties of 30×11.5-14.5, Type VIII, Aircraft Tires of Bias-Ply and Radial-Belted Design*. NASA TP-2810, 1988.
12. Lopez, Mercedes C.; Davis, Pamela A.; Vogler, William A.; and Yeaton, Robert B.: *Fore-and-Aft Stiffness and Damping Characteristics of 30×11.5-14.5, Type VIII, Bias-Ply and Radial-Belted Aircraft Tires.* SAE Paper 881357, Oct. 1988.
13. Davis, Pamela A.; and Lopez, Mercedes C.: Stiffness and Damping Characteristics of a Bias-Ply and Radial-Belted 30×11.5-14.5, Type VIII, Aircraft Tire. *Presented at the Eighth Annual Meeting and Conference on Tire Science and Technology,* (Akron, Ohio) Mar. 1989.
14. Anonymous: Aircraft Radial Tires. *TechTIP Newsl.*, No. TT88012, Aug. 31, 1988.
15. Wagner, Paul M.: *Laboratory Evaluation of the Michelin 25.5×8.0R14/18 Ply Rating Aircraft Radial Tire*. AFWAL-TM-87-205/FIEM, Aug. 1987.
16. Yager, Thomas J.; Stubbs, Sandy M.; and Davis, Pamela A.: *Aircraft Radial-Belted Tire Evaluation*. SAE Paper 901913, Oct. 1990.
17. Davis, Pamela A.: Evaluation of 26×6.6 Radial-Belted and Bias-Ply Aircraft Tires. *Presented at the Tire Industry Conference*, (Greenville, South Carolina) Oct. 1991.
18. Hooker, R. J.: *Dynamic Behaviour of Pneumatic Tyres*. BU-412, Bristol Univ., June 1990.
19. Davis, Pamela A.: *Comparison of 30×11.5-14.5 Bias-Ply and Radial-Belted Tire Characteristics.* SAE Paper 922012, Oct. 1992.
20. Davis, Pamela A.; and Lopez, Mercedes C.: *Static Mechanical Properties of 30×11.5-14.5, Type VIII, Aircraft Tires of Bias-Ply and Radial-Belted Design*. SAE Paper 871868, Oct. 1987.

21. Von Schlippe, B.; and Dietrich, R.: *Shimmying of a Pneumatic Wheel*. WPAFB F-TS-3727-RE, Oct. 1941.

22. Von Schlippe, B.; and Dietrich, R.: *Shimmying of a Pneumatic Wheel*. Papers on Shimmy and Rolling Behavior of Landing Gears Presented at Stuttgart Conference Oct. 16 and 17, 1941, NACA TM-1365, 1954, pp. 125–160.

23. Moreland, William J.: The Story of Shimmy. *J. Aeronaut. Sci*., vol. 21, no. 12, Dec. 1954, pp. 793–808.

24. de Carbon, Christian Bourcier: *Analytical Study of Shimmy of Airplane Wheels*. NACA TM-1337, 1952.

25. Collins, R. L.: Theories on the Mechanics of Tires and Their Applications to Shimmy Analysis. *J. Aircr.*, vol. 8, no. 4, April 1971, pp. 271–277.

26. Collins, R. L.; and Black, R. J.: Experimental Determination of Tire Parameters for Aircraft Landing Gear Shimmy Stability Studies. AIAA-68-311, April 1968.

27. Smiley, Robert F.: *Some Considerations of Hysteresis Effects on Tire Motion and Wheel Shimmy.* NACA TN 4001, 1957.

28. Horne, Walter B.: *Static Force-Deflection Characteristics of Six Aircraft Tires Under Combined Loading*. NACA TN 2926, 1953.

29. Tanner, John A.; Stubbs, Sandy M.; and McCarthy, John L.: *Static and Yawed-Rolling Mechanical Properties of Two, Type VII, Aircraft Tires*. NASA TP-1863, 1981.

30. Sleeper, Robert K.; and Dreher, Robert C.: *Tire Stiffness and Damping Determined From Static and Free-Vibration Tests.* NASA TP-1671, 1980.

31. Dodge, R. N.; and Clark, S. K.: *Comparison of Some Static and Dynamic Mechanical Properties of 18×5.5 and 49×17 Type VII Aircraft Tires as Measured by Three Test Facilities*. NASA CR-165720, 1981.

32. Harvay, Gabriel; and Crowe, R. E.: *Spring and Damping Constants of Helicopter Tires*. McDonnell Aircraft Corp., H-122-1, July 17, 1945.

33. Clark, S. K.; Dodge, R. N.; and Nybakken, G. H.: Dynamic Properties of Aircraft Tires. *J. Aircr.*, vol. 11, no. 3, Mar. 1974, pp. 166–172.

34. Thompson, A. G.: The Effect of Tyre Damping on the Performance of Vibration Absorbers in an Active Suspension. *J. Sound & Vib.*, vol. 133, no. 3, 1989, pp. 457–465.

35. Brahney, James H., ed.: Radial Tires for Aircraft? *Aerosp. Eng.*, May 1988, pp. 21–23.

36. Panikkar, T. P. K.: Dunlop Aircraft Radial Tyres. *Dunlop Aerosp. Group Newsl.*, vol. 2, no. 3, Aug. 1986.

37. Hutton, David V.: *Applied Mechanical Vibrations*. McGraw-Hill, 1981, pp. 59–69.

38. Meirovitch, Leonard: *Elements of Vibration Analysis.* McGraw-Hill, 1975, pp. 1–87.

39. Meirovitch, Leonard: *Analytical Methods in Vibrations*. MacMillian Co., 1967, pp. 1–123, 388–390.

40. Thomson, William Tyrrell: *Theory of Vibration with Applications.* Prentice-Hall, Inc., 1972, pp. 1–78.

41. Horne, Walter B.; and Dreher, Robert C.: *Phenomena of Pneumatic Tire Hydroplaning*. NASA TN D-2056, 1963.

42. Horne, Walter B.; Yager, Thomas J.; and Ivey, Don L.: Recent Studies to Investigate Effects of Tire Footprint Aspect Ratio on Dynamic Hydroplaning Speed. *The Tire Pavement Interface, STEM STEP 929*, M. G. Potting and T. J. Yager, eds., ASTM, 1986.

Table 1. Characteristics of 30×11.5-14.5/26PR Aircraft Tires

Parameter	Bias-ply	Radial-belted
Size	30×11.5-14.5	30×11.5-14.5
Ply rating	26	26
Weight, lb	68.75	55.50
Rated vertical load, lb	25000	25000
Rated inflation pressure at 35-percent load deflection, psi	245	310
Outside diameter of unloaded tire, in.	30	30
Maximum carcass width of unloaded tire, in.	8	8
Tread grooves	3	4

Table 2. Viscous Damping Parameters

Symbol	Definition
$\zeta = \frac{\delta}{\sqrt{2\pi^2 - \delta^2}}$	Viscous damping factor
$\zeta = \frac{\delta}{2\pi}$	Viscous damping factor for small δ
$\delta = \ln\frac{x_1}{x_2}$	Log decrement
$\omega_d = \omega_n\sqrt{1-\zeta^2}$	Damped frequency of oscillation
$k = m\omega_n^2 = m\left(\frac{2\pi}{\tau}\right)^2$	Spring rate

Table 3. Structural Damping Parameters

Symbol	Definition
$\beta = 2\zeta$	Structural damping factor
$C_{\text{eq}} = \frac{\beta k}{\omega}$	Equivalent viscous damping factor
$\delta = \ln\frac{x_1}{x_2} \cong \pi\beta$	Log decrement
$\Delta E_{\text{cyc}} = \pi\beta k X^2$	Energy loss per cycle
$k = m\omega_n^2 = m\left(\frac{2\pi}{\tau}\right)^2$	Spring rate
$\omega_d = \omega_n\sqrt{1-\zeta^2}$	Damped frequency of oscillation

Table 4. Coulomb Friction Parameters

Symbol	Definition
$F_d = \mu_k W$	Damping or friction force
$f_d = \frac{F_d}{k}$	Equivalent displacement
$k = \frac{2F_d}{2X}$	Spring rate

Table 5. Quasi-static and Dynamic Lateral Load Test Data

Tire	Maximum deflection, in.	Spring rate, lb/in.		Structural damping	Viscous damping	Energy loss, in-lb	
		Slope	Axis			Measurement	Calculation
Quasi-static data:							
Bias	0.38	10622	7214	0.042	—	289	319
Radial	0.52	8098	5674	0.038	—	300	339
Dynamic data:							
Bias	0.32	—	7585	0.092	0.047	—	217
Radial	0.37	—	6676	0.062	0.031	—	175

Table 6. Static and Dynamic Fore-and-Aft Load Test Data

Tire	Maximum deflection, in.	Spring rate, lb/in.		Structural damping	Viscous damping	Energy loss, in-lb	
		Slope	Axis			Measurement	Calculation
Quasi-static data:							
Bias	0.19	26495	16145	0.068	—	229	222
Radial	0.27	15833	9394	0.044	—	169	128
Dynamic data:							
Bias	0.14	—	20610	0.172	0.086	—	204
Radial	0.16	—	11025	0.128	0.064	—	136

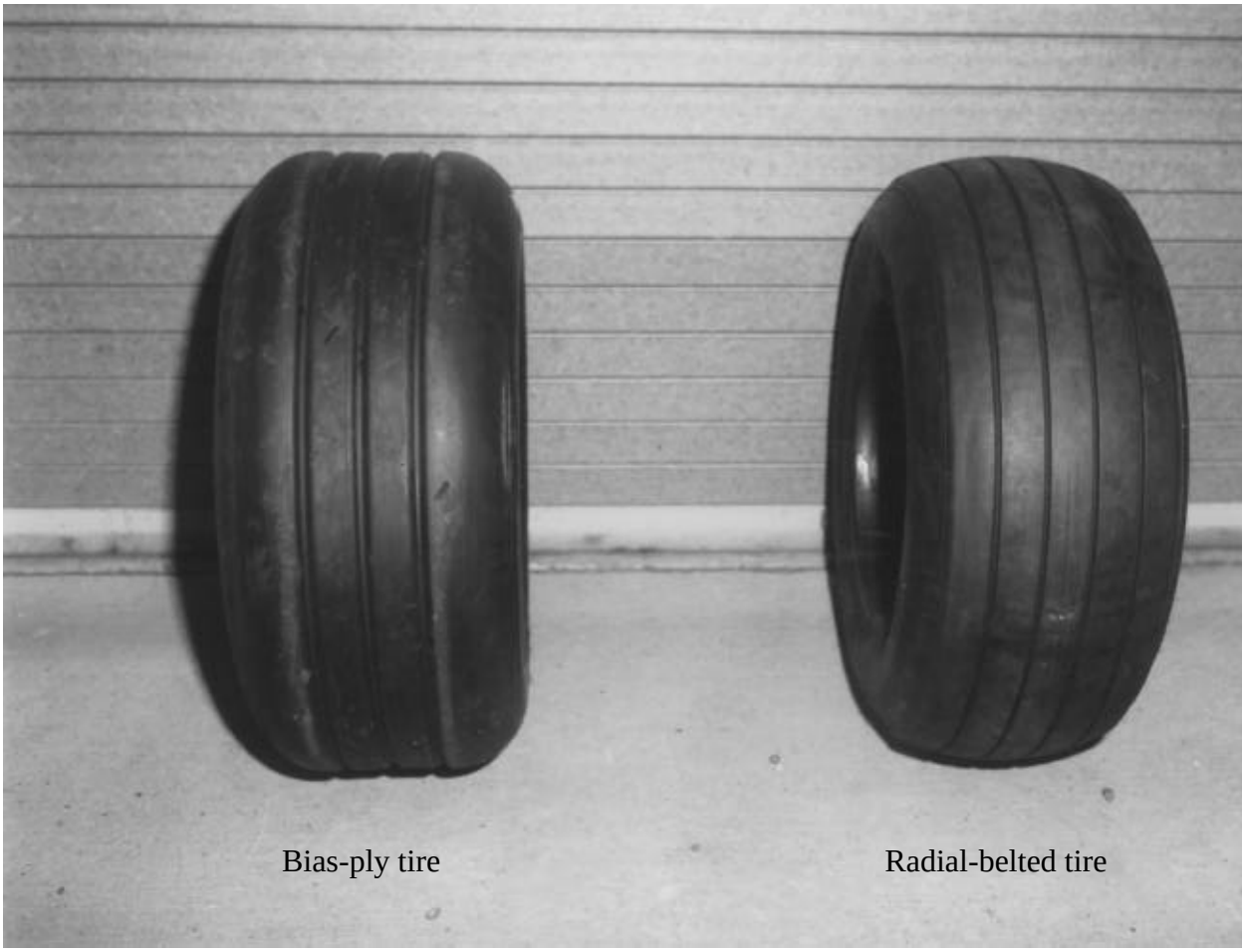

L-86-10,087

Figure 1. The 30×11.5-14.5/26PR aircraft tires.

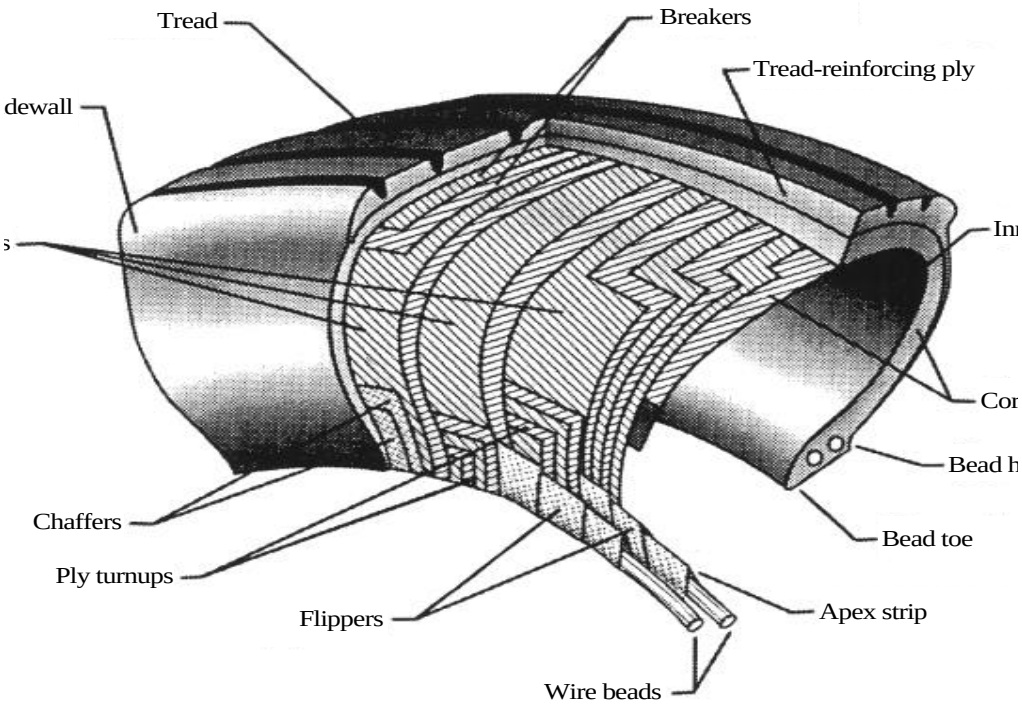

Figure 2. Bias-ply aircraft tire construction.

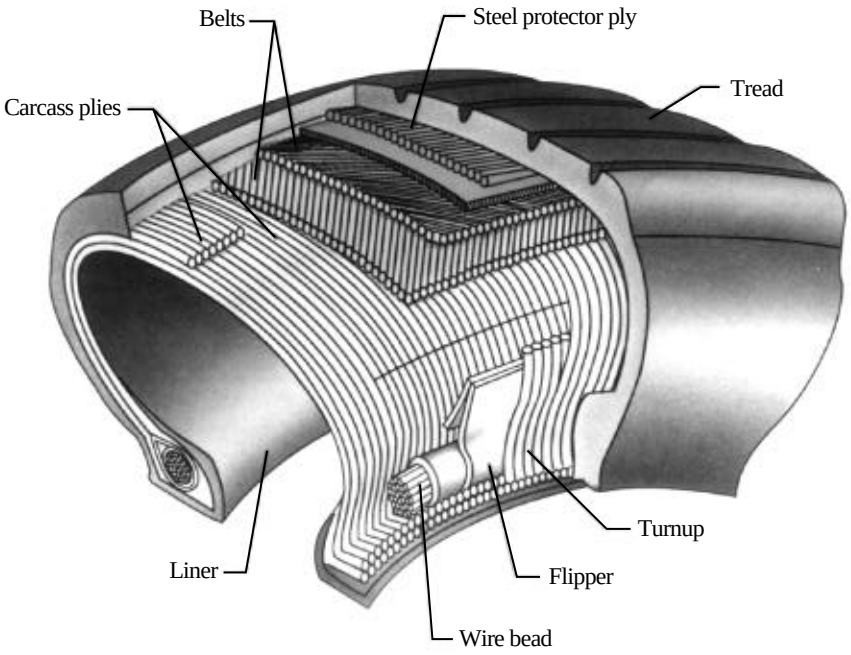

Figure 3. Radial-belted aircraft tire construction.

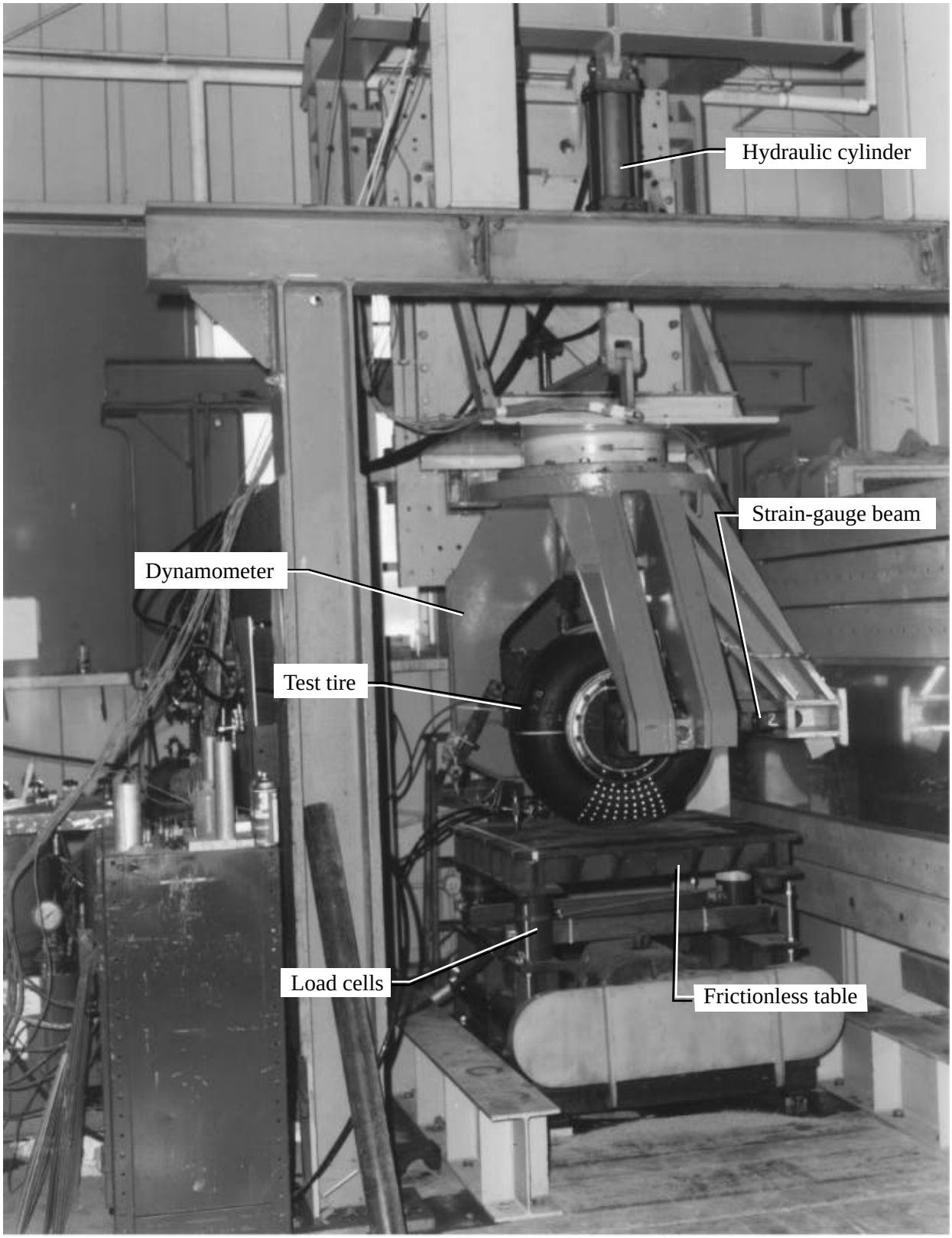

L-86-174

Figure 4. Test apparatus no. 1 (used for quasi-static vertical load tests).

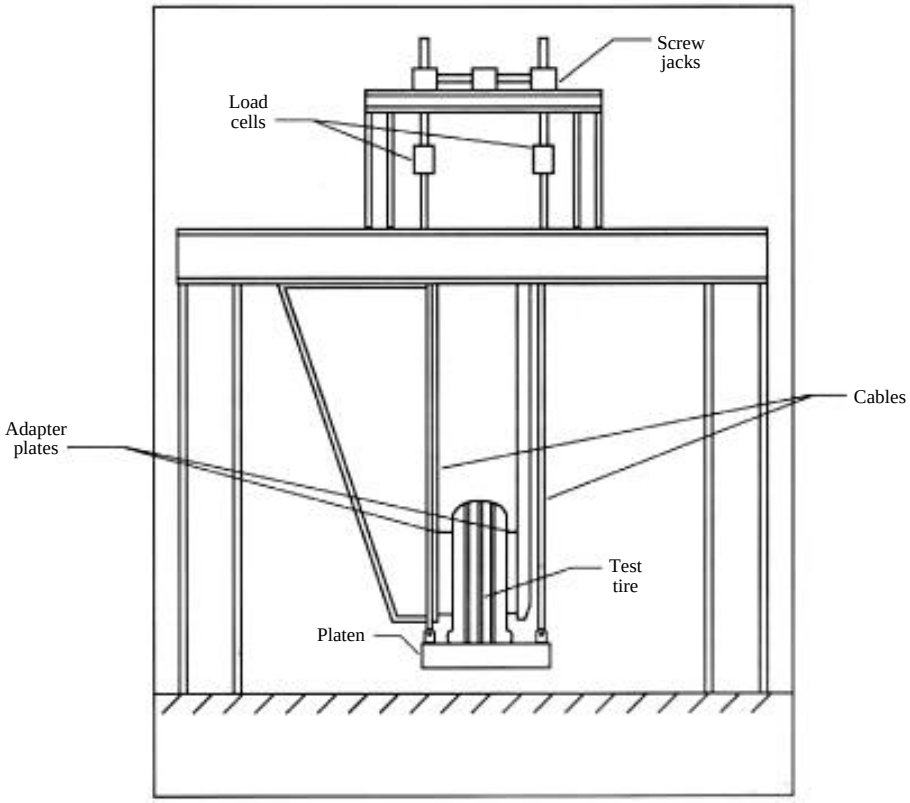

Figure 5. Test apparatus no. 2 (used for quasi-static and dynamic lateral and fore-and-aft load tests).

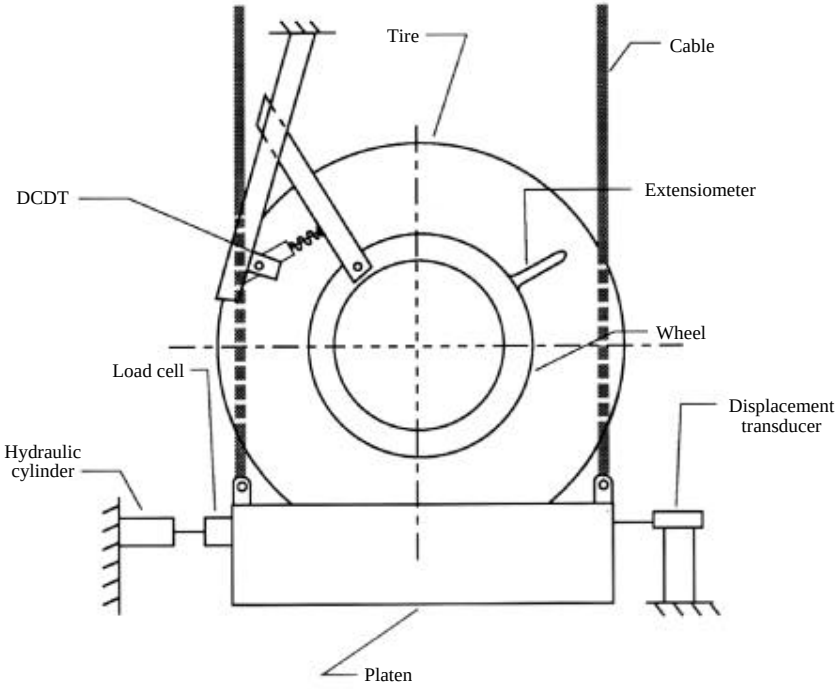

Figure 6. Quasi-static fore-and-aft test setup for test apparatus no. 2.

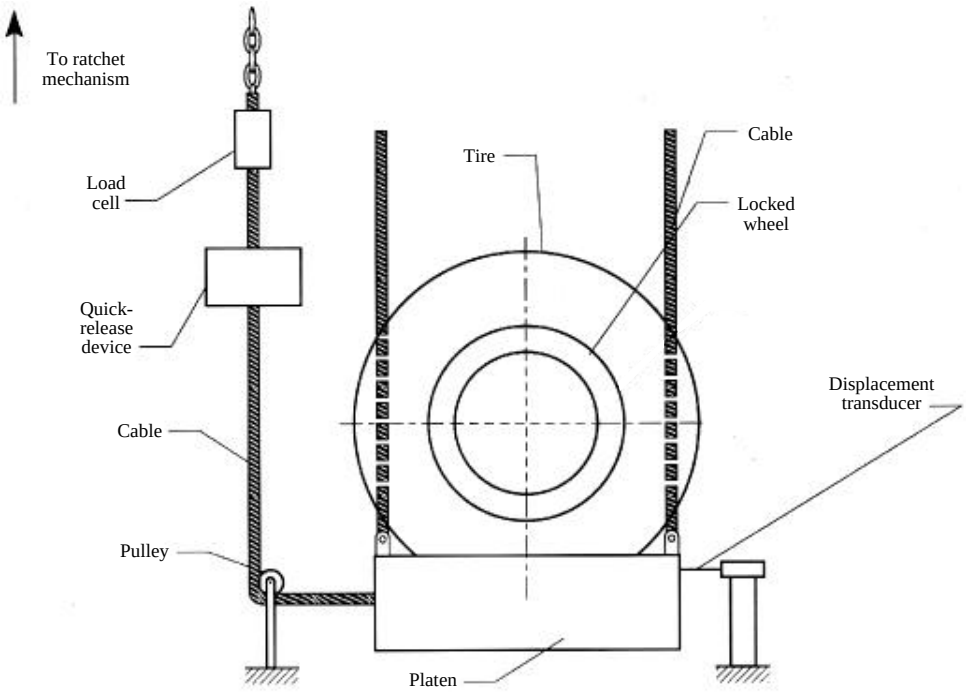

Figure 7. Free-vibration fore-and-aft test setup for test apparatus no. 2.

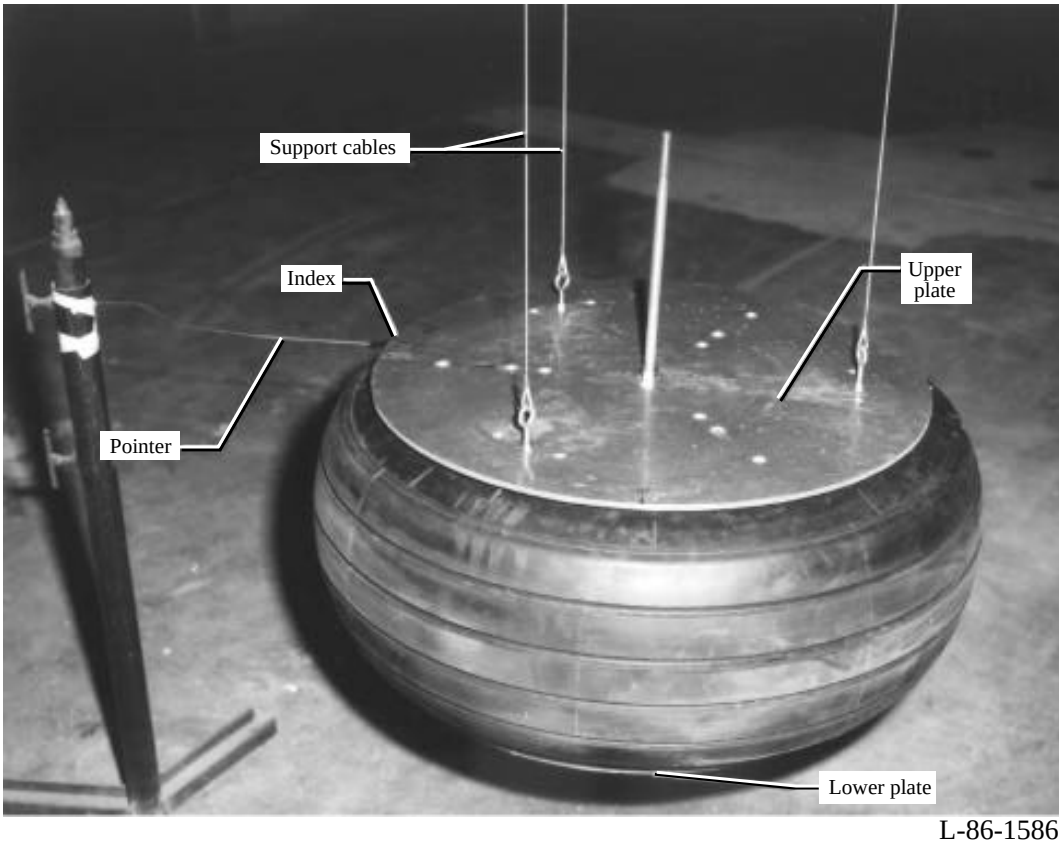

L-86-1586

Figure 8. Torsional pendulum apparatus used for moment-of-inertia tests.

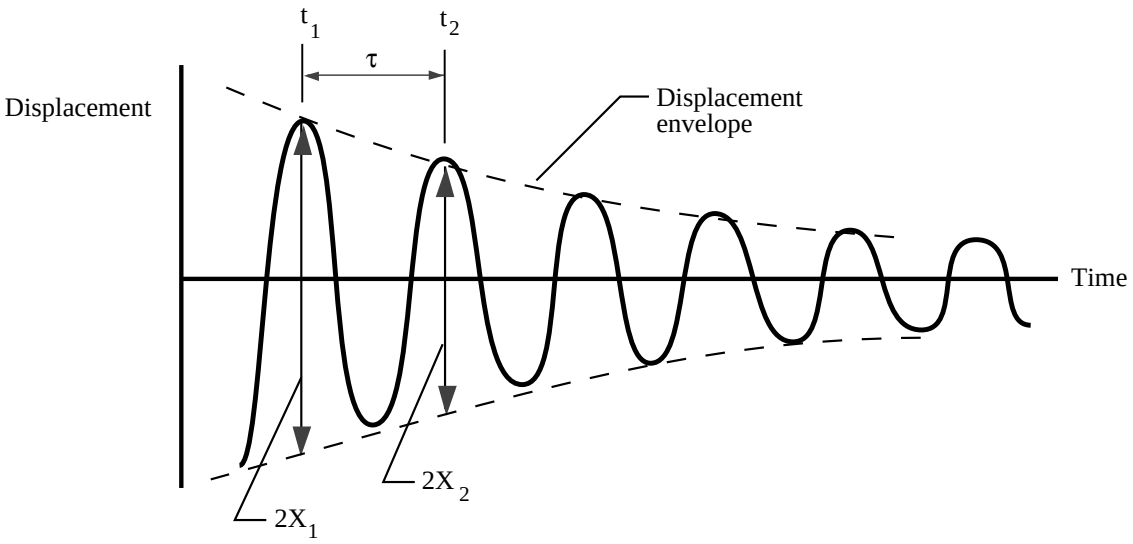

Figure 9. Response of underdamped system, $0 < \zeta < 1$.

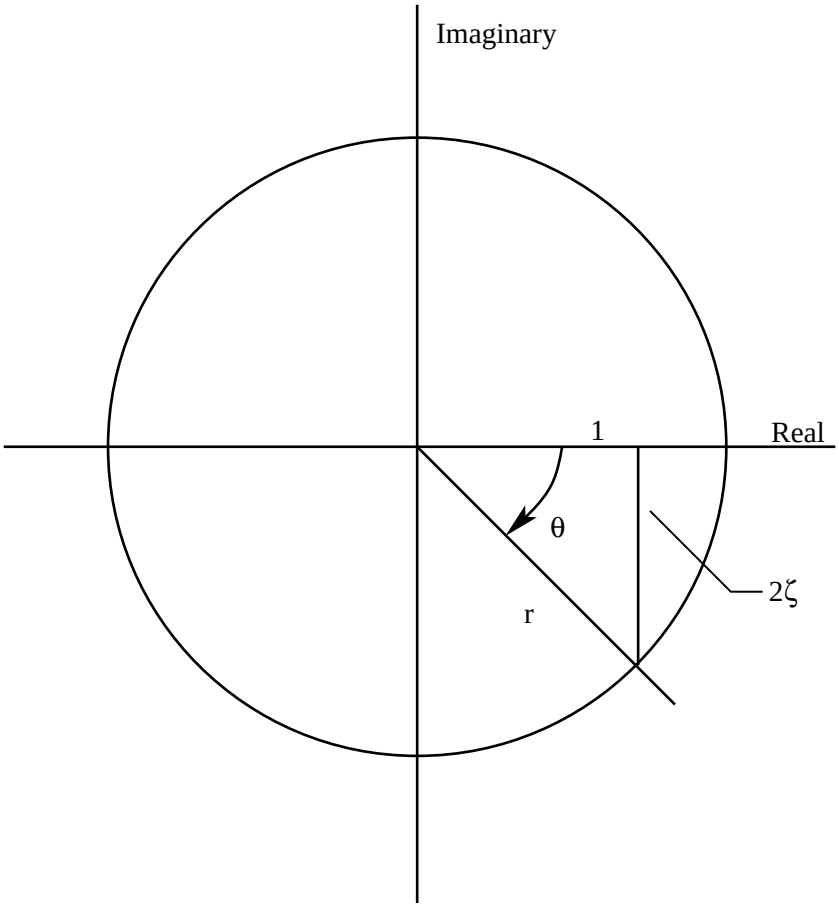

Figure 10. Polar notation of damping parameter.

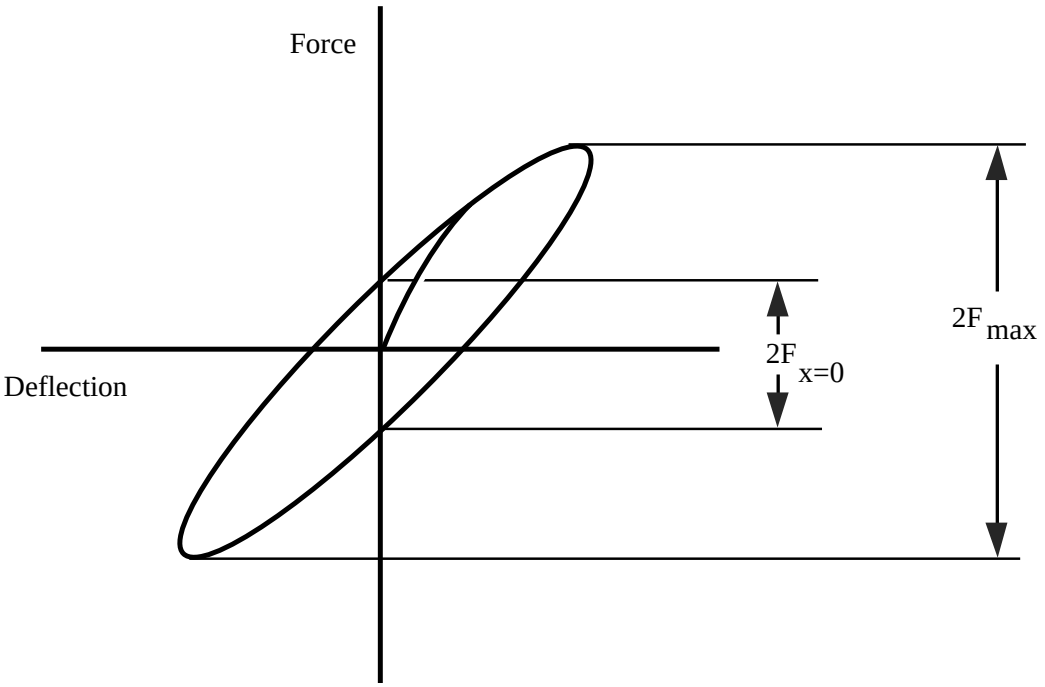

Figure 11. Quasi-static damping factor components.

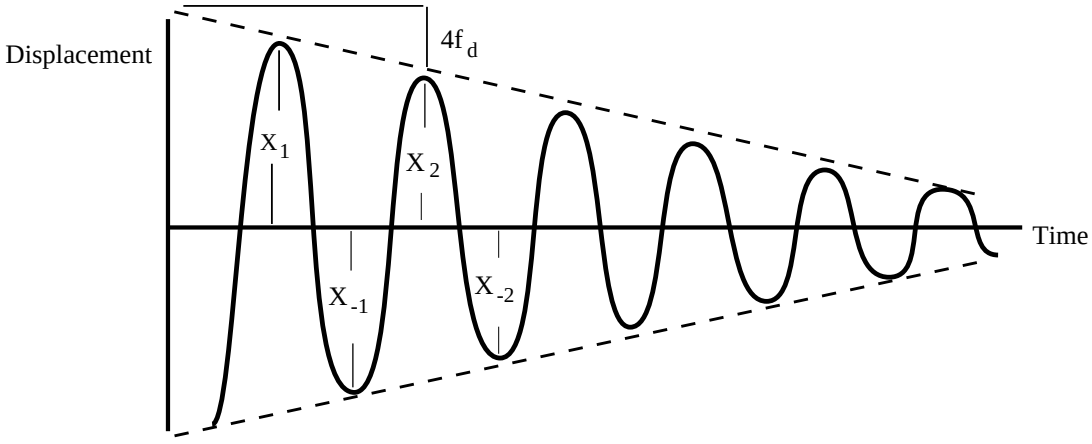

Figure 12. Response of system with Coulomb friction.

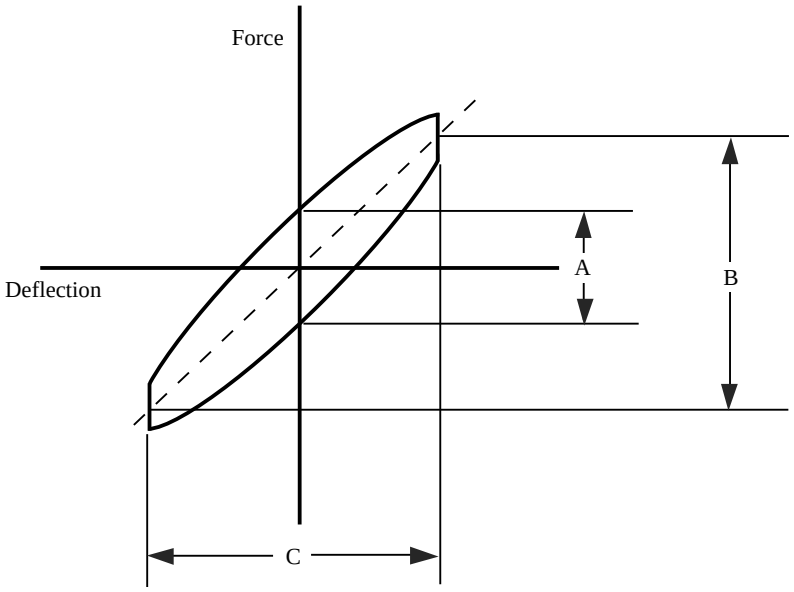

Figure 13. Response of system under quasi-static load with Coulomb friction.

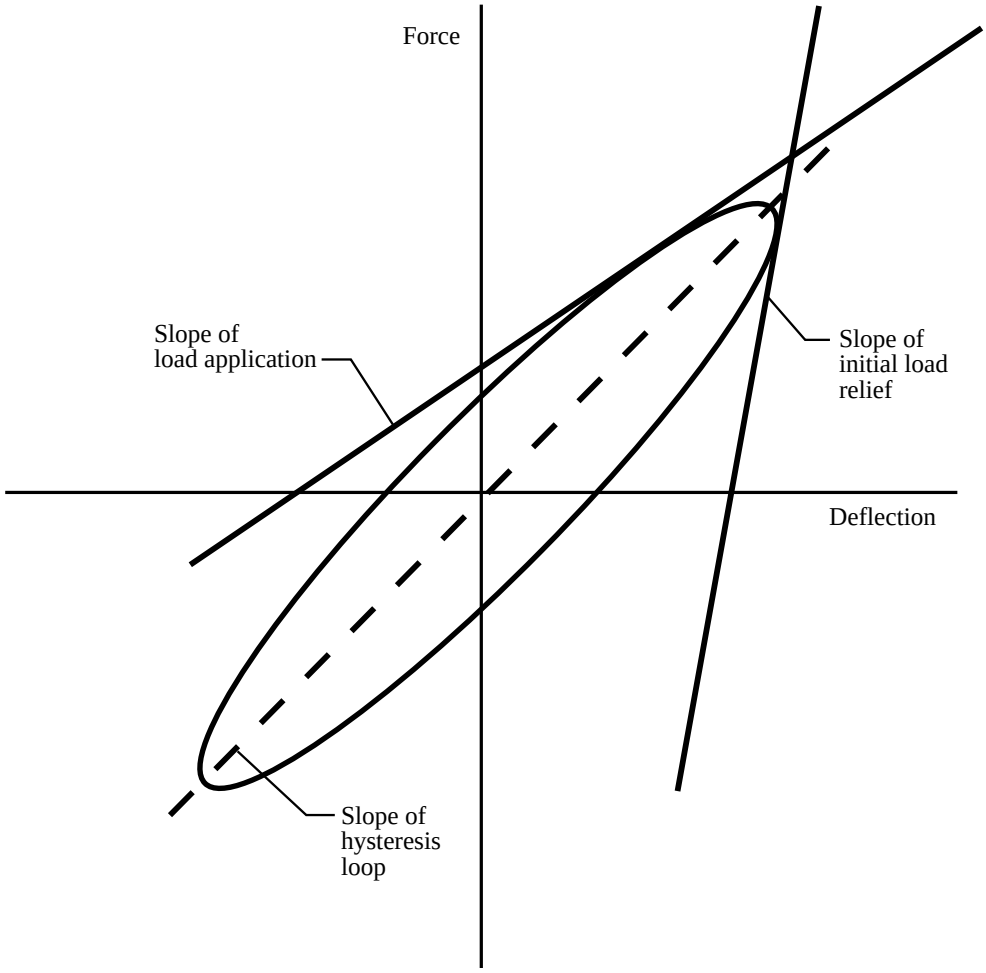

Figure 14. Spring rate defined by hysteresis loop.

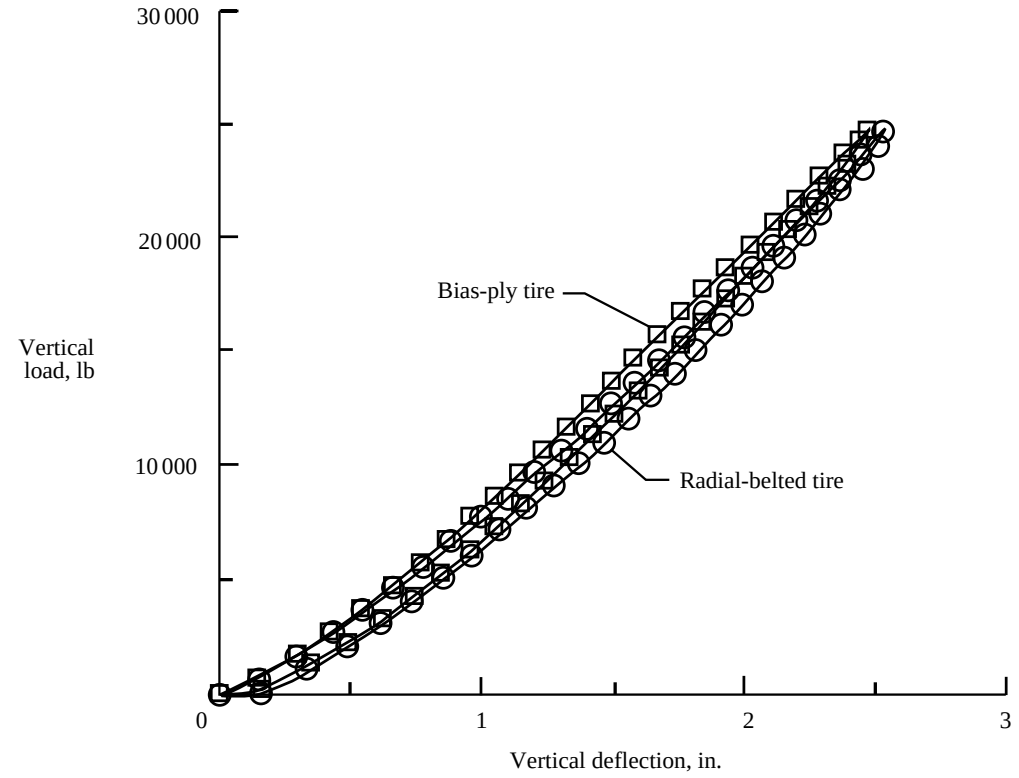

Figure 15. Vertical load-deflection curve of bias-ply and radial-belted tires.

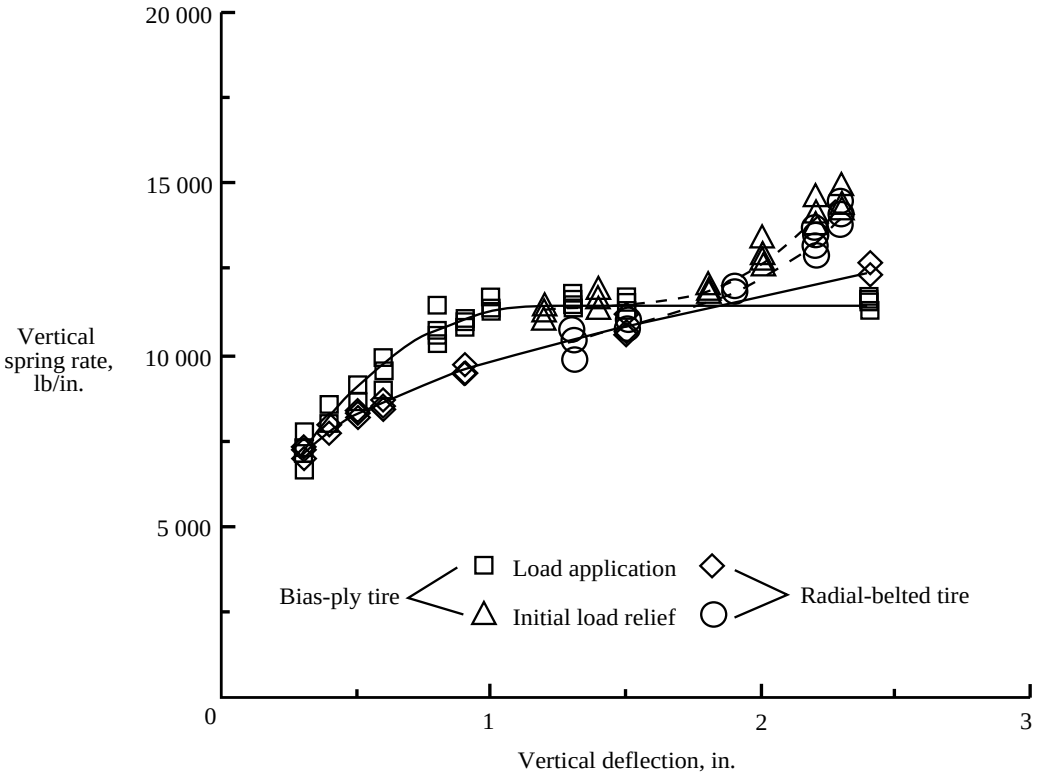

Figure 16. Vertical stiffness characteristics of bias-ply and radial-belted tires.

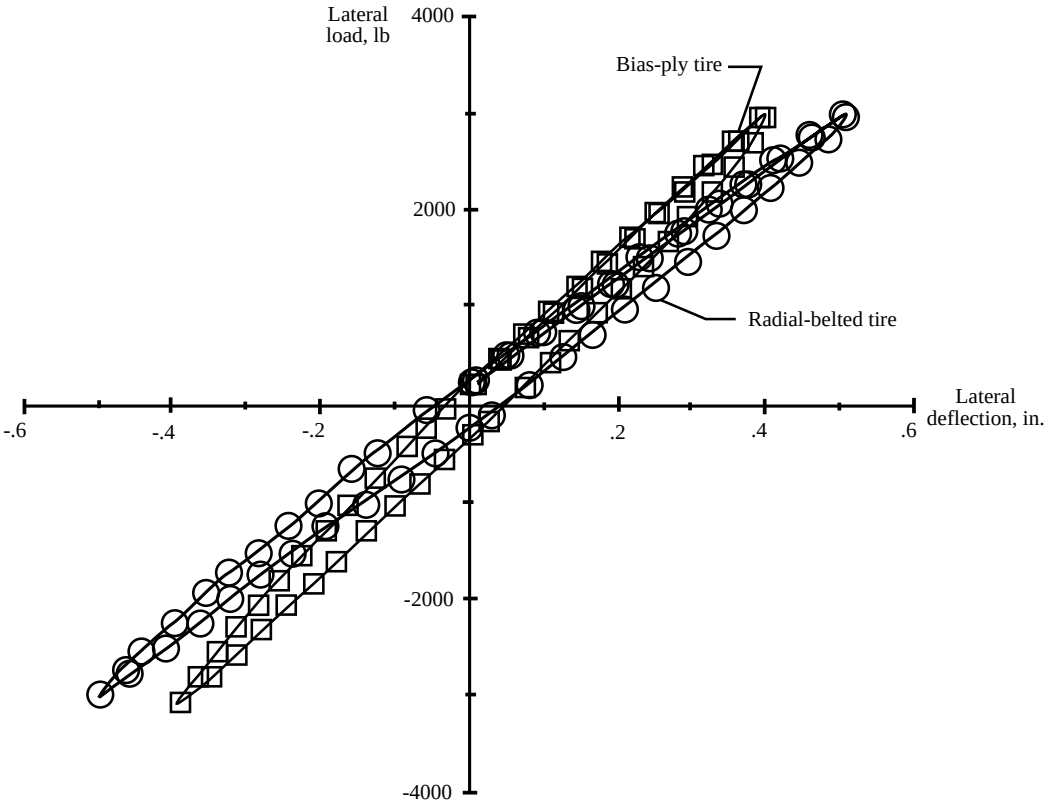

Figure 17. Lateral load-deflection curve of bias-ply and radial-belted tires.

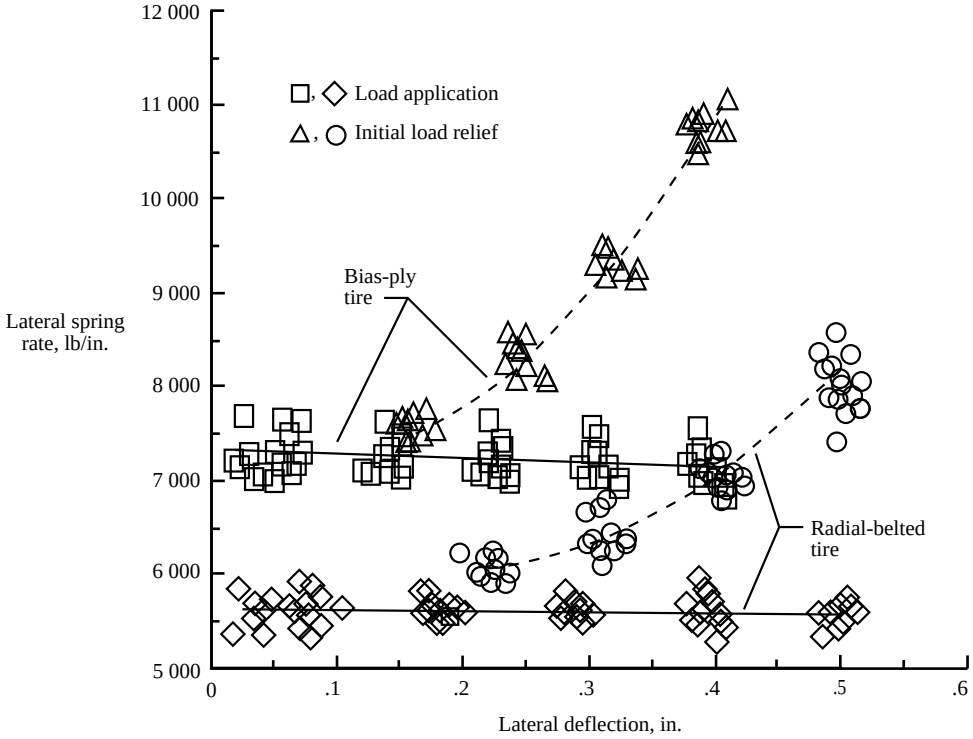

Figure 18. Lateral stiffness characteristics of bias-ply and radial-belted tires.

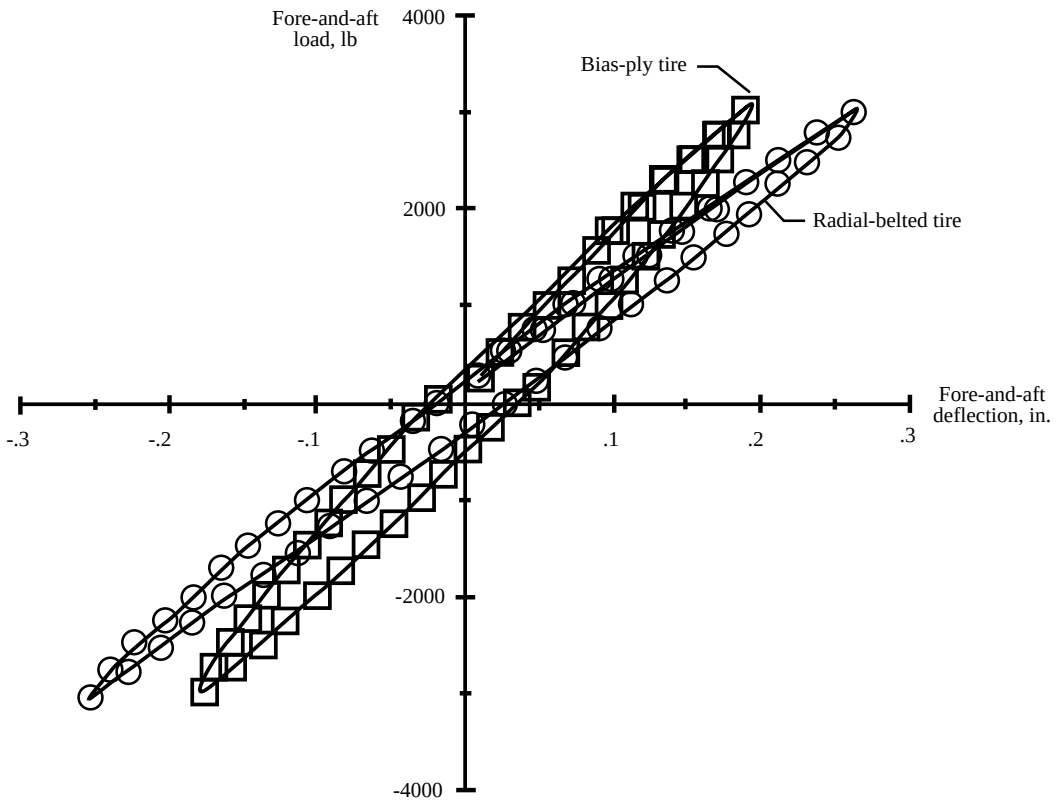

Figure 19. Fore-and-aft load-deflection curve of bias-ply and radial-belted tires.

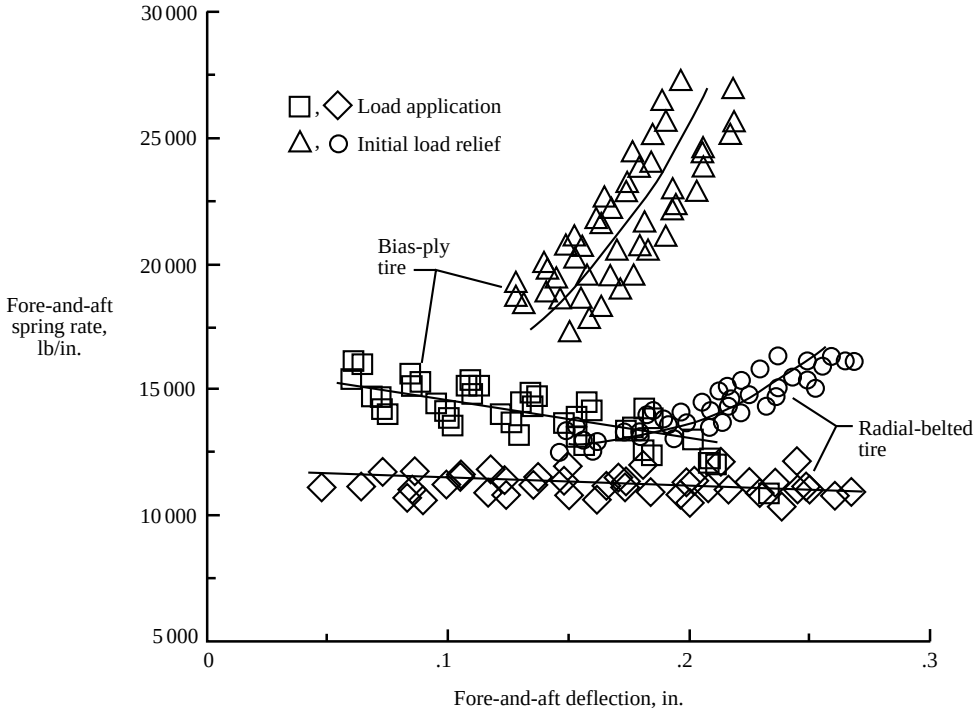

Figure 20. Fore-and-aft stiffness characteristics of bias-ply and radial-belted tires.

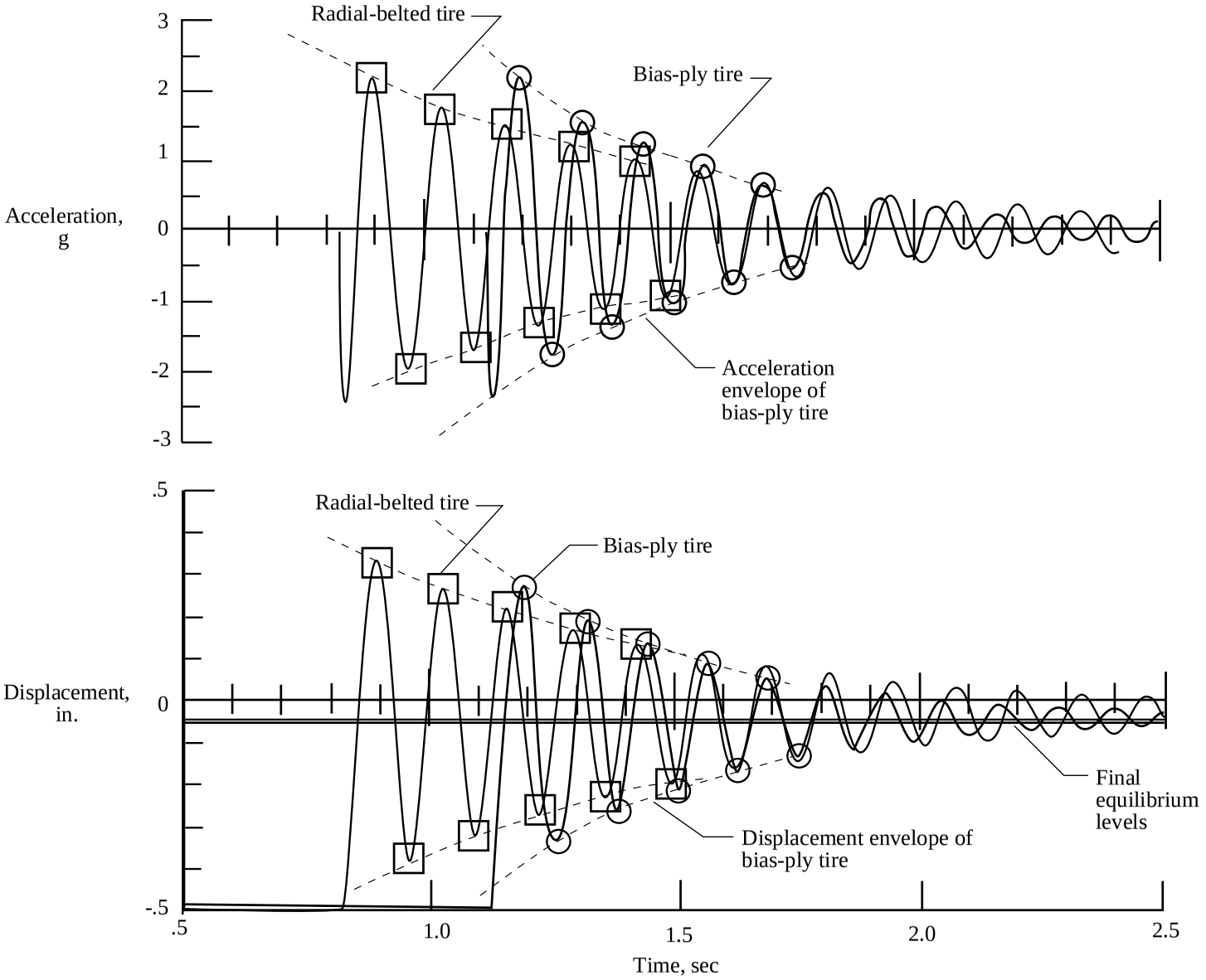

Figure 21. Lateral free-vibration time-history plots of bias-ply and radial-belted tires.

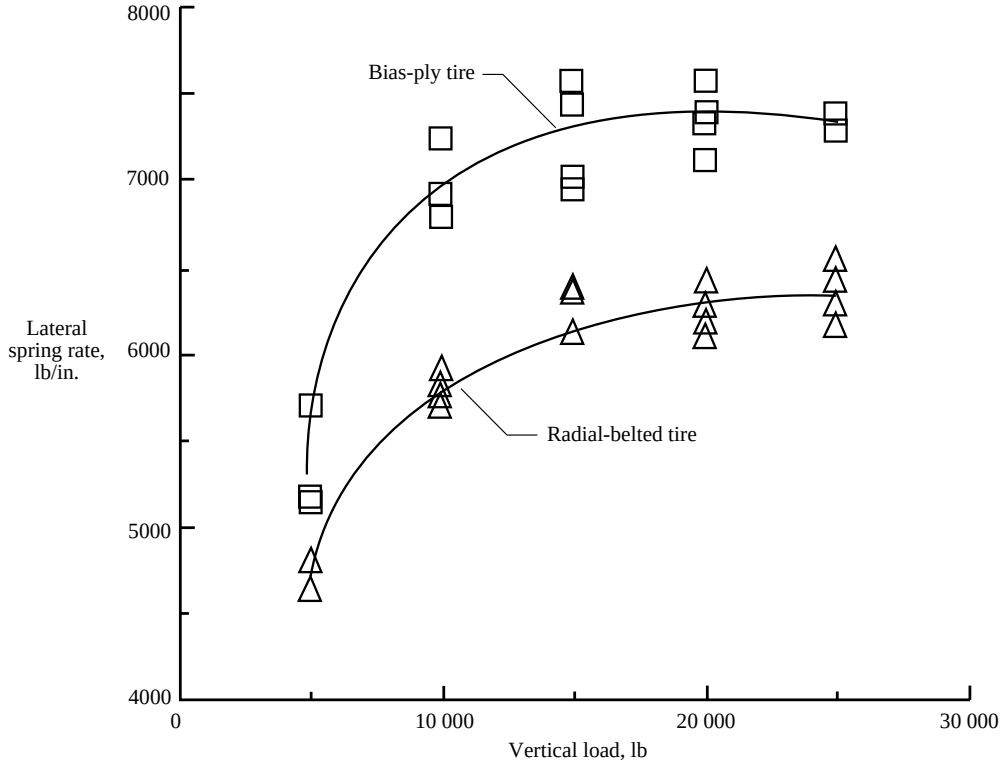

Figure 22. Lateral free-vibration stiffness characteristics of bias-ply and radial-belted tires.

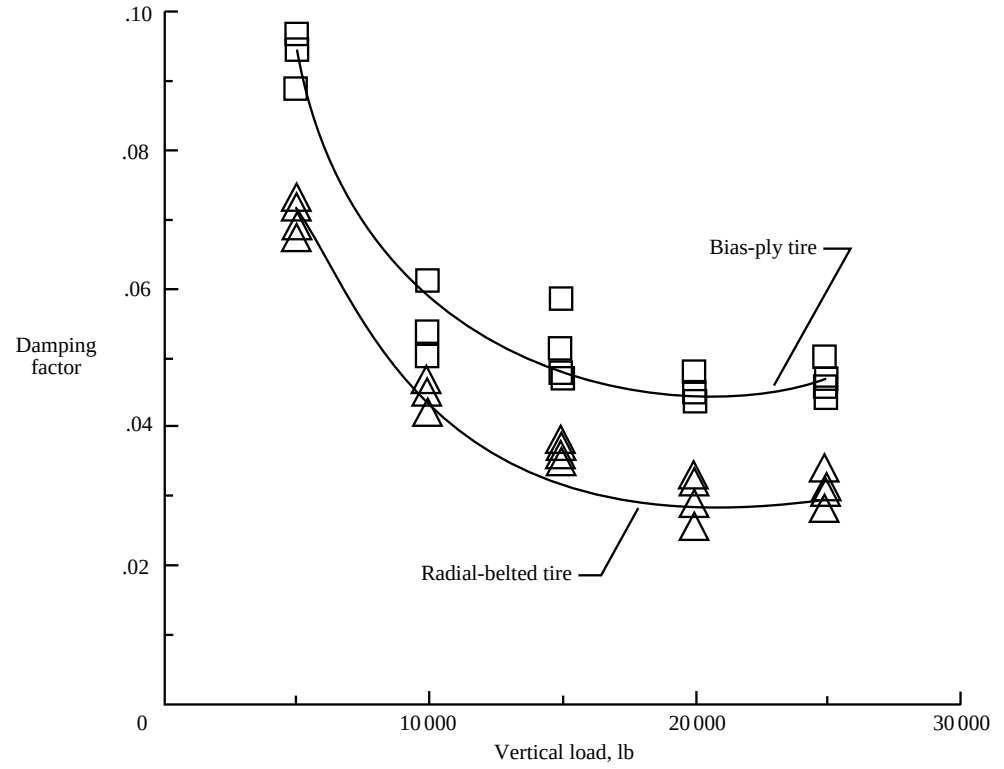

Figure 23. Lateral free-vibration damping characteristics of bias-ply and radial-belted tires.

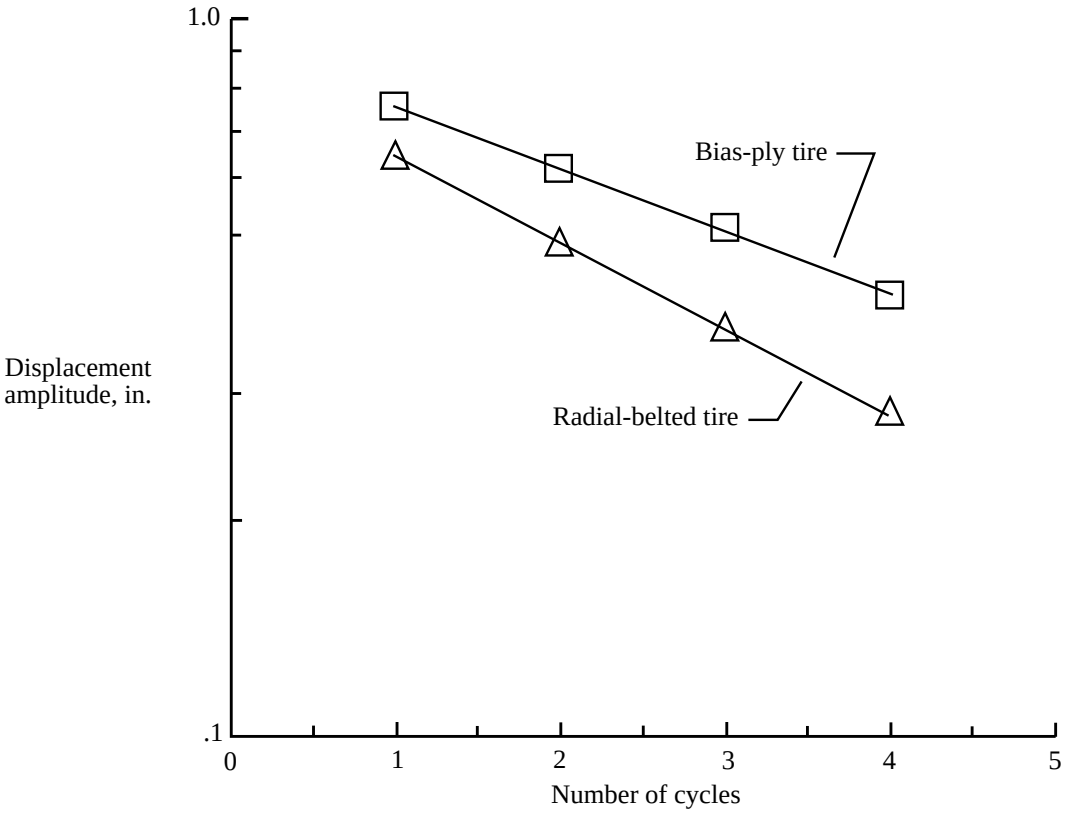

Figure 24. Frequency effects of displacement amplitude.

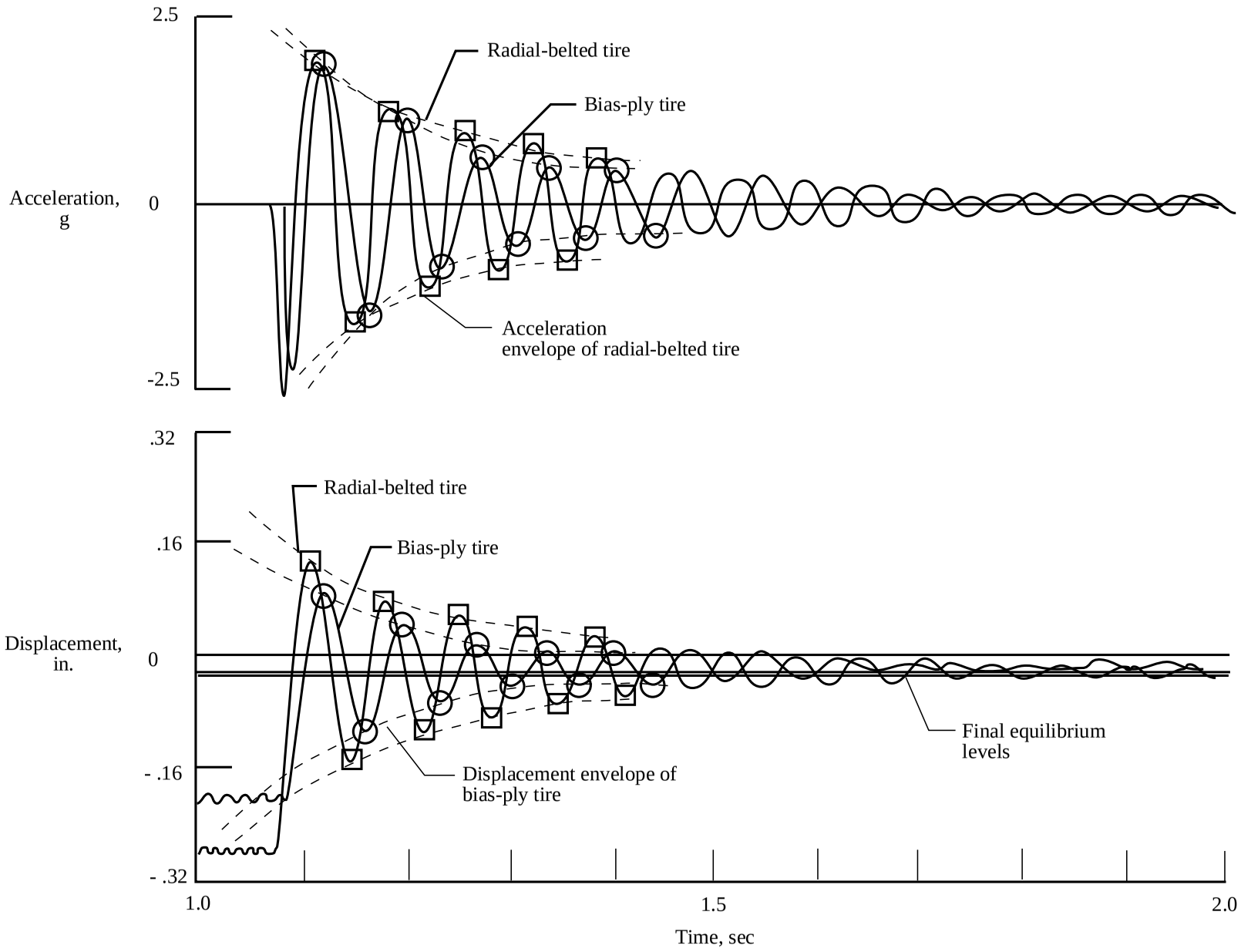

Figure 25. Fore-and-aft free-vibration time-history plots of bias-ply and radial-belted tires.

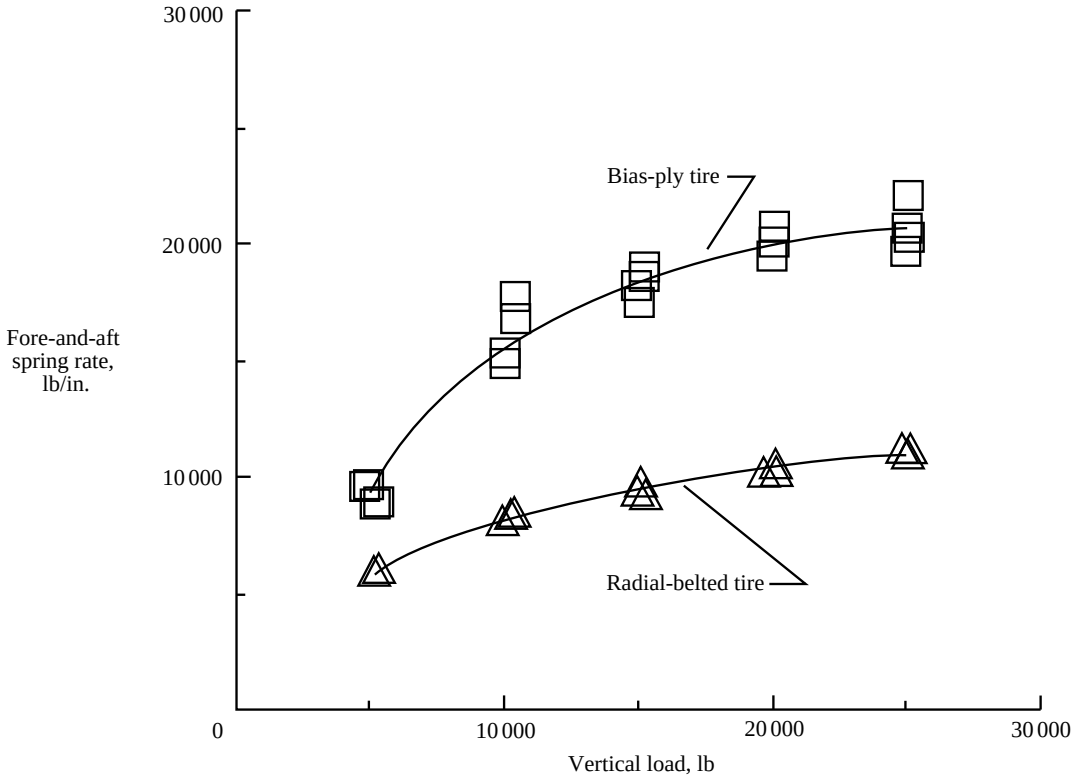

Figure 26. Fore-and-aft free-vibration stiffness characteristics of bias-ply and radial-belted tires.

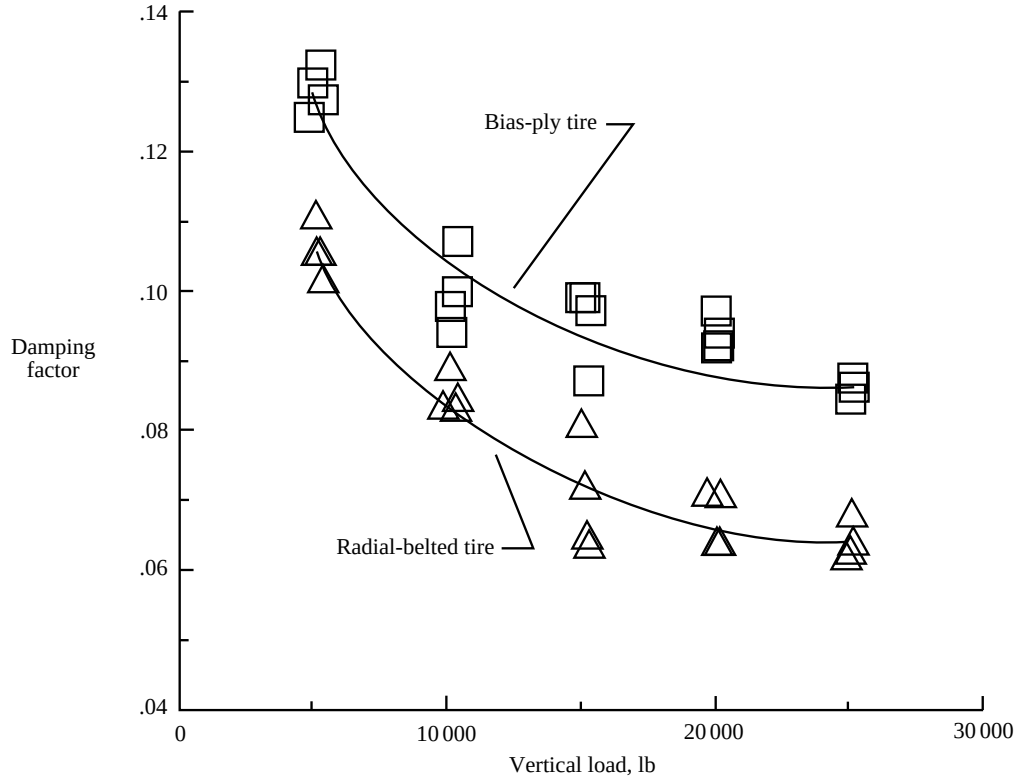

Figure 27. Fore-and-aft free-vibration damping characteristics of bias-ply and radial-belted tires.

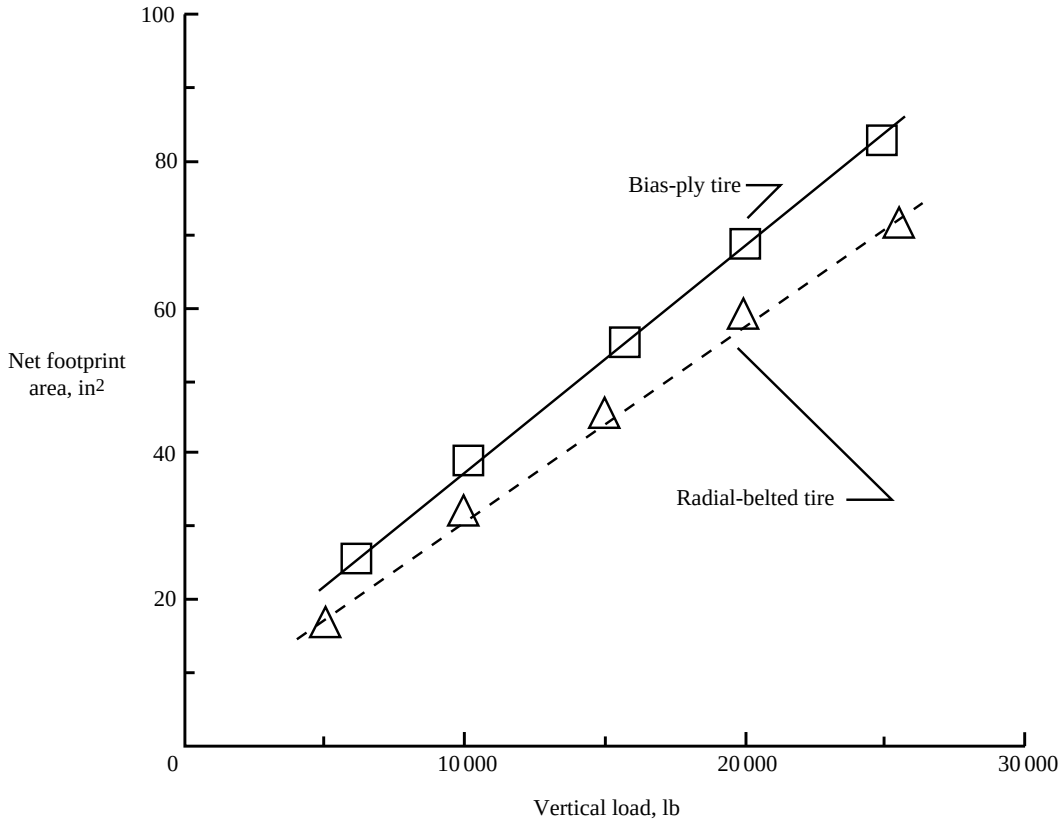

Figure 28. Net tire footprint area as function of vertical load of bias-ply and radial-belted tires.

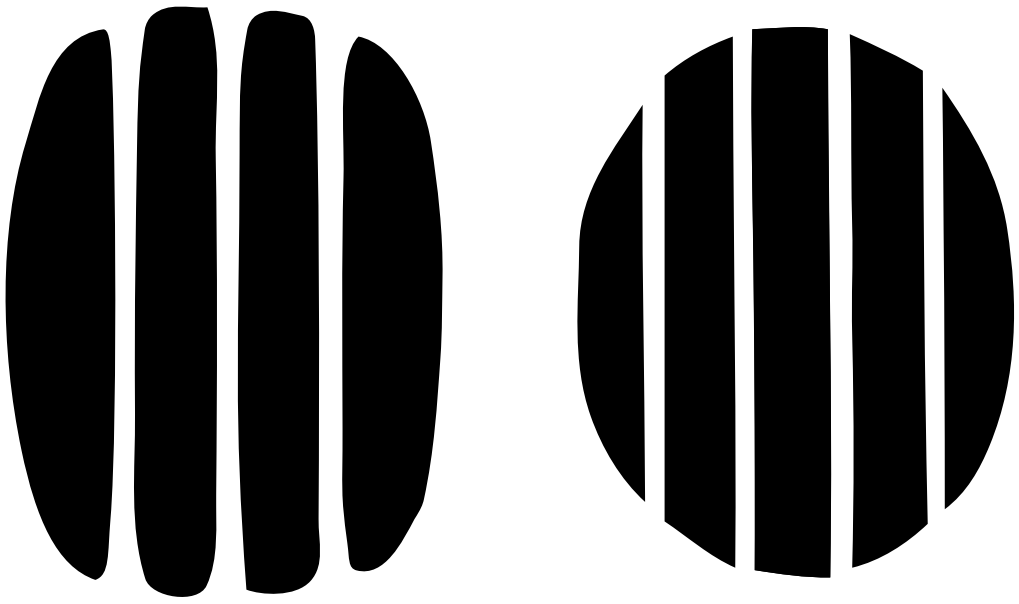

Bias-ply tire Radial-belted tire

Figure 29. The 30×11.5-14.5/26PR tire footprint silhouettes at 25000-lb vertical load.

REPORT DOCUMENTATION PAGE

Form Approved
OMB No. 0704-0188

1. AGENCY USE ONLY *(Leave blank)*	2. REPORT DATE	3. REPORT TYPE AND DATES COVERED
	February 1997	Technical Paper

4. TITLE AND SUBTITLE
Quasi-Static and Dynamic Response Characteristics of F-4 Bias-Ply and Radial-Belted Main Gear Tires

5. FUNDING NUMBERS
WU 505-63-10-02

6. AUTHOR(S)
Pamela A. Davis

7. PERFORMING ORGANIZATION NAME(S) AND ADDRESS(ES)
NASA Langley Research Center
Hampton, VA 23681-0001

8. PERFORMING ORGANIZATION REPORT NUMBER
L-17433

9. SPONSORING/MONITORING AGENCY NAME(S) AND ADDRESS(ES)
National Aeronautics and Space Administration
Washington, DC 20546-0001

10. SPONSORING/MONITORING AGENCY REPORT NUMBER
NASA TP-3586

11. SUPPLEMENTARY NOTES

12a. DISTRIBUTION/AVAILABILITY STATEMENT
Unclassified–Unlimited
Subject Category 05
Availability: NASA CASI (301) 621-0390

12b. DISTRIBUTION CODE

13. ABSTRACT *(Maximum 200 words)*

An investigation was conducted at Langley Research Center to determine the quasi-static and dynamic response characteristics of F-4 military fighter 30×11.5-14.5/26PR bias-ply and radial-belted main gear tires. Tire properties were measured by the application of vertical, lateral, and fore-and-aft loads. Mass moment-of-inertia data were also obtained. The results of the study include quasi-static load-deflection curves, free-vibration time-history plots, energy loss associated with hysteresis, stiffness and damping characteristics, footprint geometry, and inertia properties of each type of tire. The difference between bias-ply and radial-belted tire construction is given, as well as the advantages and disadvantages of each tire design. Three simple damping models representing viscous, structural, and Coulomb friction are presented and compared with the experimental data. The conclusions discussed contain a summary of test observations.

14. SUBJECT TERMS	15. NUMBER OF PAGES
Radial belted; Bias-ply; Aircraft tires; Hysteresis; Free vibration; Load deflection; Energy loss; Footprint geometry; Damping; Stiffness	42
	16. PRICE CODE: A03

17. SECURITY CLASSIFICATION OF REPORT	18. SECURITY CLASSIFICATION OF THIS PAGE	19. SECURITY CLASSIFICATION OF ABSTRACT	20. LIMITATION OF ABSTRACT
Unclassified	Unclassified	Unclassified	